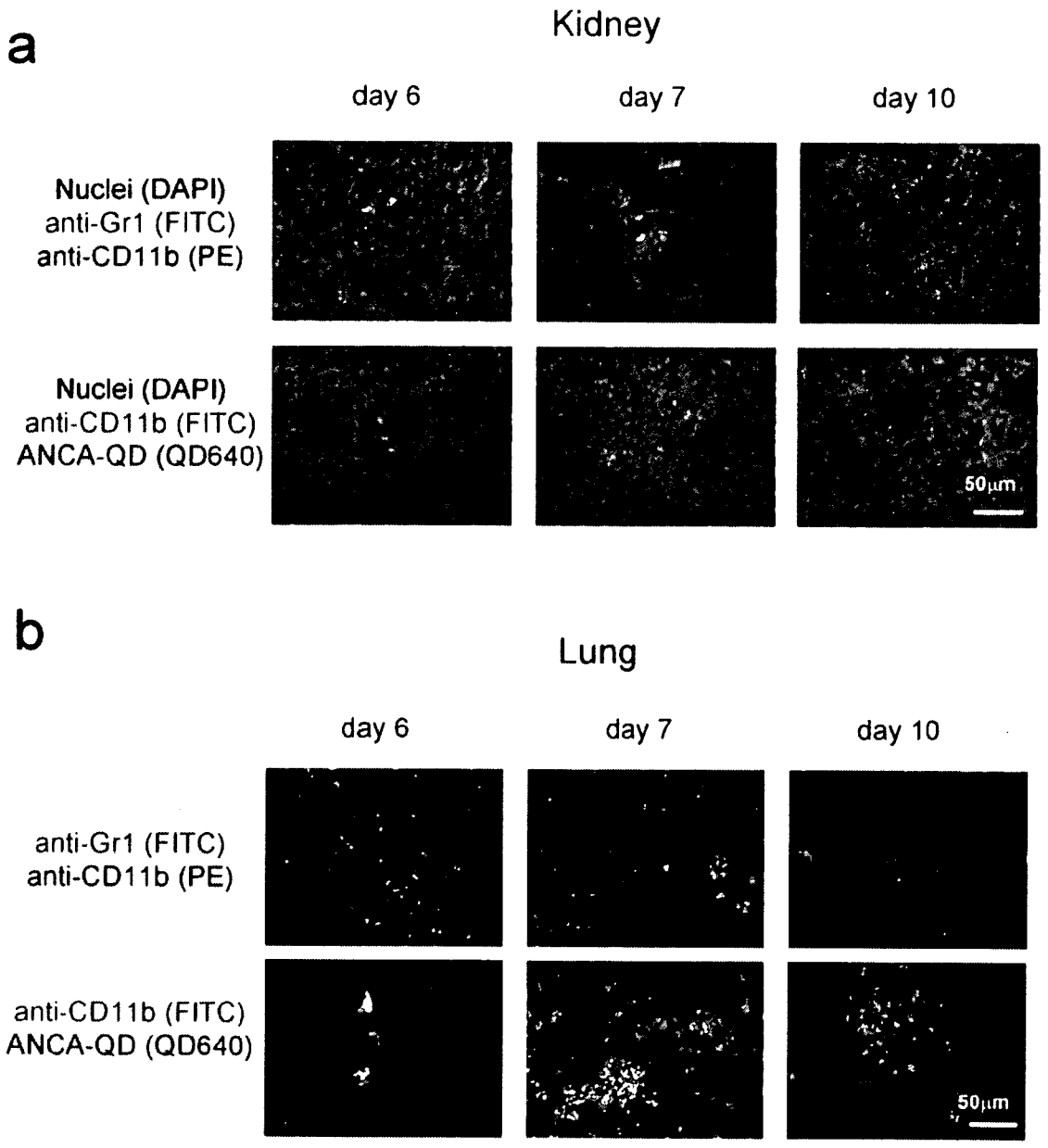

Fig. 8. ANCA-QD in renal glomerular lesion and pulmonary aggregation with infiltrated $CD11b^+$ and $Gr1^+$ neutrophils. Immunohistochemical stain of kidney and lung cryosections in mice receiving MPO-ANCA (1 mg of naïve Ab with an additional 250 μg/ml of ANCA-QD for imaging). *a*, Kidney lesion including injured glomeruli was collected on days 6, 7, and 10, then embedded in frozen sections and sliced to 4-μm thickness. The cryosection was stained with FITC anti-Gr1, PE anti-CD11b Ab (upper) and FITC anti-CD11b Ab (lower). ANCA-QD accumulated on the glomerular lesion was observed with fluorescent microscopy with a long-pass filter (>610-nm wavelength). The cryosection was stained with DAPI to display the location of the glomerulus. QD-positive cells were located around glomeruli. Original magnification, ×400. Bar indicates 50 μm. *b*, Injured lung collected on days 6, 7, and 10 was stained with FITC anti-Gr1, PE anti-CD11b Abs (upper), and FITC anti-CD11b Ab (lower), as described above. Large clusters of $CD11b^+$ and QD^+ are present in lung of day 10.

Table 1. Serum cytokine production of SCG/Kj mice

Cytokine conc. (pg/ml)	Control C57BL/6J	Anti-MPO treated C57BL/6J mice Day 5	Anti-MPO treated C57BL/6J mice Day 7	SCG/Kj
IL-1β	111.18 ± 13.44	141.01 ± 3.54	157.06 ± 7.78	207.41 ± 1.41
TNF-α	51.69 ± 9.65	169.46 ± 7.07	164.29 ± 8.49	1,064.07 ± 141.42
IL-6	12.56 ± 29.7	192.40 ± 21.92	547.33 ± 5.66	181.11 ± 63.64
IL-12(p40)[a]	4.77 ± 9.90	440.1 ± 19.8	302.35 ± 48.08	1,233.17 ± 115.26
IL-12(p70)[b]	21.52 ± 17.68	101.41 ± 33.94	90.54 ± 8.49	6.87 ± 0.71
IL-17	10.20 ± 7.78	39.81 ± 8.49	83.79 ± 5.66	106.58 ± 73.54
KC (CXCL1)	63.47 ± 18.31	783.7 ± 54.45	779.20 ± 88.39	414.7 ± 12.73
RANTES	264.59 ± 20.51	1,181.21 ± 84.85	940.52 ± 202.23	989.89 ± 137.18
G-CSF	42.77 ± 72.83	3,079.11 ± 113.14	461.43 ± 169.00	3,399.56 ± 111.72

The serum cytokine level of mice with MPO-ANCA-induced systemic vasculitis at the indicated time and that of SCG/Kj mice was measured by the Bio-Plex® cytokine detection kit. C57BL/6J mice were pretreated with CAWS and MPO-ANCA twice on days 0 and 5, as described in "Materials and Methods" (n=4). Serum cytokines of aged SCG/Kj mice developing glomerulonephritis (13 wks, male, n=4). The data are presented as the mean ± standard deviation of duplicate samples (n=4).

[a] IL-12p40 is detected by anti-IL-12p40 antibody.

[b] IL-12p70 is detected by the combination of anti-IL-12p35 and anti-IL-12p40 antibodies.

MPO-ANCA were not directly associated with the activated neutrophil. This is consistent with our previous results that MPO-ANCA was directly bound with glomerular endothelium and upregulated some adhesion molecules, including ICAM-1, VCAM-1, and E-selectin (35). In contrast, ANCA-QD was highly accumulated to the $CD11b^+$ macrophage cluster in lung inflammatory lesion (Fig. 8b). These results suggested that the infiltrated neutrophils in kidney and pulmonary lesion play a significant role in systemic vasculitis progression and inflammation. MPO-ANCA might act directly not to the neutrophils but to other cells, including mesangial and pulmonary epithelial cells.

Increased Cytokine Production in ANCA-Induced Systemic Vasculitis

Next, we investigated whether the serum cytokine level was increased and correlated with the neutrophil activations, because we have already revealed that neutrophils were activated and translocated MPO on membrane surface. Therefore, we exhaustively analyzed 18 kinds of cytokine production by Bioplex® analysis. Serum cytokine levels were dramatically changed with the development of vascular lesion. Proinflammatory cytokines, including IL-6, IL-1β and TNF-α and some neutrophil-related chemokines and growth factor including G-SCF, RANTES, and KC (murine functional IL-8), were significantly increased (Table 1). The anticipated secondary stimulants to activate neutrophils were due to those elevated cytokines such as G-CSF and RANTES that were released in response to the innate defense and subsequently drove some adhesion molecules, including integrin molecules and some chemokines, which was induced by belatedly produced cytokines such as IL-6. These results suggested that costimulation with MPO-ANCA and CAWS mannoprotein induce the neutrophil activation with MPO membrane translocation due to the produced proinflammatory cytokines.

Discussion

Several groups have examined that the histopathological features of systemic vasculitis caused in mice by stimulation with *C. albicans*-derived glycoprotein and the principal genetic roles in the development of coronary arterial vasculitis (36). It has also been reported that enzymatic activity of serum MPO level was elevated in neutrophils and marked higher ANCA titers in *Candida*-induced coronary vasculitis mice, similar to the same features in SCG/Kj mice (38). In addition, the ANCA titer is dramatically diminished in MPO-deficient mice (3, 19), indicating that fungal infection has relevance to the MPO molecule. Evidence suggests that MPO is an essential enzyme to protect fungal infection, and the overactivation of MPO could be a risk factor for arterial vasculitis formation. In the present study, we established a novel systemic vasculitis model by combination of mimicked higher ANCA titer by MPO-ANCA and mimicked fungal infection by CAWS. The fact that high levels of MPO-ANCA resulted in kidney dysfunction is consistent with the clinical feature that patients with ANCA-related RPGN showed significantly increased MPO activity and MPO-ANCA titer (14). These results suggest that the MPO-ANCA significantly participates in glomerulonephritis

in both mouse and human.

We have previously demonstrated that neutrophilic enzymatic activity is enhanced by stimulation with FMLP and proinflammatory cytokines. MPO was believed to exist not on the surface but inside neutrophils and seemed to leak MPO and other lysosomal peroxidase from the granules when neutrophils were activated (24). However, no direct evidence was observed to leak MPO on the neutrophil surface during neutrophil activation, whereas expression of PR3 on the surface of the primed neutrophils can be detected (4, 13, 50). The detection of MPO translocation on living neutrophils by QD is nothing short of groundbreaking. We assumed that the neutrophils in patients with ANCA-associated RPGN were constitutively activated by higher levels of proinflammatory cytokines and serum MPO. Our observation that neutrophils in patients translocate MPO on their surface without any stimulation supports this hypothesis. It is noteworthy that some healthy controls show lower MPO translocation on the surface of neutrophils even in unstimulated conditions in our experiments, and the ratio of MPO-translocated neutrophils also varied among patients and even in healthy controls. Similar features are also reported by PR3 expression levels on the surface of activated neutrophils; PR3 expression levels varied significantly in patients and even in healthy controls (44–46). These results indicate that resident translocation levels of MPO might be involved in the potential risk for developing MPO-ANCA-associated RPGN.

Visualization of MPO-ANCA in the early phase of systemic vasculitis by ANCA-QD provided a good deal of information about the initiation of neutrophil-mediated inflammation. Several researchers have noted that higher titers of ANCA mediate neutrophil responses in vascular inflammation directly and indirectly (5). Massive systemic inflammation, including nephritis and pulmonary hemorrhage, was observed with specific accumulation of ANCA-QD. Especially in kidney, immunohistochemical staining showed that neutrophils located around the fringe of glomeruli with the development of mesangiolysis. To support this, we have previously reported that MPO-ANCA directly bound to primary glomerular endothelium following upregulation of ICAM-1, VCAM-1, E-selectin, and promotion of TNF-α production (35). These results are consistent with the observation of Little et al. (31) that MPO-ANCA on leukocytes interacts with vascular endothelium via ICAM-1 in systemic vasculitis rats with developed MPO-ANCA. We also observed severe oliguria subsequently due to the mesangioproliferation with capillary obstruction on the glomeruli. The interaction among neutrophils, endothelium and MPO-ANCA promotes cytokine production from endothelial and/or mesangial cells around infiltrated neutrophil in the glomeruli, resulting in epithelial cell lysis, including mesangiolysis and interstitial hemorrhage, and consequently systemic vasculitis (40, 41, 43).

We hypothesized that the developmental time course of this systemic vasculitis seemed to be stepwise : 1) CAWS induced neutrophil priming following cytokine production with ANCA, 2) ANCA mediated neutrophil/endothelium activation. We demonstrated that peritoneal neutrophils have a potential to respond to MPO-ANCA and induce proinflammatory cytokines. MPO-ANCA and CAWS cooperatively promotes the production of proinflammatory cytokines, including IL-1, IL-6, IL-8 (in human), and TNF-α by a subset of macrophages and epithelial cells (27). However, we observed no MPO translocation on the neutrophil surface despite CAWS stimulation, implying that stimulation with only CAWS is insufficient to initiate neutrophil activation. Furthermore, CAWS have an ability to induce IL-6 by peritoneal neutrophils, subsequently resulting in enhanced neutrophil activation on day 7. In addition to CAWS, MPO-ANCA also might be contributed to neutrophil activation, because in our systemic vasculitis model we injected MPO-ANCA to mimic a higher ANCA titer just as in human RPGN patients, but CAWS alone failed to induce proinflammatory cytokine production (data not shown). In addition, only administration of MPO-ANCA promotes a lower level of IL-12p40 and G-CSF production (data not shown), implying a higher ANCA titer than in conventional conditions is a trigger to induce proinflammatory cytokine production in response to fungal infection. These results suggested that cytokine production in this model was promoted by at least two separate pathways: via MPO-ANCA specific activation and the CAWS-mediated pathway. A higher ANCA titer, established by repeated fungal infection, may be a potential risk for a patient who has a hereditary factor for autoimmune disease onset.

We conclude that the initial step of systemic vasculitis is due to the enhanced activation of neutrophils by CAWS and MPO-ANCA. CAWS and MPO-ANCA cooperatively trigger neutrophil activation by producing proinflammatory cytokines.

This work was supported primarily by grants from the Ministry of Health, Labour and Welfare, Japan and the Program for Promotion of Fundamental Studies in Health Sciences of the Organization for Pharmaceutical Safety and Research, Japan (K. Suzuki), by a grant from the Japan Health Sciences Foundation on "Research on Health Sciences focusing on Drug Innovation, International Collaborative Research" (H. Hashimoto), partially

by a grant from Medical Techniques Promotion Research (H14-nano-004) from the Ministry of Health, Labour and Welfare, Japan (K. Yamamoto), and also partially by a grant for young researchers from the Japan Foundation of Cardiovascular Research (A. Hoshino). The author thanks Dr. Taeko Dohi (Department of Gastroenterology, Research Institute, International Medical Center of Japan), Dr. Yasuhiro Natori, and Ms. Mikiko Uwano (Department of Clinical Pharmacology, Research Institute, IMCJ) for kind and valuable advice and for help with the histochemical experiments on kidney.

References

1) Aratani, Y., Kura, F., Watanabe, H., Akagawa, H., Takano, Y., et al. 2002. Critical role of myeloperoxidase and nicotinamide adenine dinucleotide phosphate-oxidase in high-burden systemic infection of mice with *Candida albicans*. J. Infect. Dis. **185**: 1833–1837.
2) Aratani, Y., Kura, F., Watanabe, H., Akagawa, H., Takano, Y., et al. 2002. Relative contributions of myeloperoxidase and NADPH-oxidase to the early host defense against pulmonary infections with *Candida albicans* and *Aspergillus fumigatus*. Med. Mycol. **40**: 557–563.
3) Aratani, Y., Kura, F., Watanabe, H., Akagawa, H., Takano, Y., et al. 2000. Differential host susceptibility to pulmonary infections with bacteria and fungi in mice deficient in myeloperoxidase. J. Infect. Dis. **182**: 1276–1279.
4) Ben-Smith, A., Dove, S.K., Martin, A., Wakelam, M.J., and Savage, C.O. 2001. Antineutrophil cytoplasm autoantibodies from patients with systemic vasculitis activate neutrophils through distinct signaling cascades: comparison with conventional Fcgamma receptor ligation. Blood **98**: 1448–1455.
5) Csernok, E. 2003. Anti-neutrophil cytoplasmic antibodies and pathogenesis of small vessel vasculitides. Autoimmun. Rev. **2**: 158–164.
6) Csernok, E., Ernst, M., Schmitt, W., Bainton, D.F., and Gross, W.L. 1994. Activated neutrophils express proteinase 3 on their plasma membrane *in vitro* and *in vivo*. Clin. Exp. Immunol. **95**: 244–250.
7) Dubertret, B., Skourides, P., Norris, D.J., Noireaux, V., Brivanlou, A.H., and Libchaber, A. 2002. *In vivo* imaging of quantum dots encapsulated in phospholipid micelles. Science **298**: 1759–1762.
8) El Messaoudi, K., Verheyden, A.M., Thiry, L., Fourez, S., Tasiaux, N., et al. 2002. Human recombinant myeloperoxidase antiviral activity on cytomegalovirus. J. Med. Virol. **66**: 218–223.
9) Fujii, A., Tomizawa, K., Arimura, Y., Nagasawa, T., Ohashi, Y.Y., et al. 2000. Epitope analysis of myeloperoxidase (MPO) specific anti-neutrophil cytoplasmic autoantibodies (ANCA) in MPO-ANCA-associated glomerulonephritis. Clin. Nephrol. **53**: 242–252.
10) Gao, X., Cui, Y., Levenson, R.M., Chung, L.W., and Nie, S. 2004. *In vivo* cancer targeting and imaging with semiconductor quantum dots. Nat. Biotechnol. **22**: 969–976.
11) Gross, W.L., Schmitt, W.H., and Csernok, E. 1993. ANCA and associated diseases: immunodiagnostic and pathogenetic aspects. Clin. Exp. Immunol. **91**: 1–12.
12) Hamano, Y., Tsukamoto, K., Abe, M., Sun, G.D., Zhang, D., et al. 2006. Genetic dissection of vasculitis, myeloperoxidase-specific antineutrophil cytoplasmic autoantibody production, and related traits in spontaneous crescentic glomerulonephritis-forming/Kinjoh mice. J. Immunol. **176**: 3662–3673.
13) Harper, L., Cockwell, P., Adu, D., and Savage, C.O. **2001**. Neutrophil priming and apoptosis in anti-neutrophil cytoplasmic autoantibody-associated vasculitis. Kidney Int. **59**: 1729–1738.
14) Harper, L., Radford, D., Plant, T., Drayson, M., Adu, D., and Savage, C.O. 2001. IgG from myeloperoxidase-anti-neutrophil cytoplasmic antibody-positive patients stimulates greater activation of primed neutrophils than IgG from proteinase 3-antineutrophil cytosplasmic antibody-positive patients. Arthritis Rheum. **44**: 921–930.
15) Heeringa, P., Huugen, D., and Tervaert, J.W. 2005. Anti-neutrophil cytoplasmic autoantibodies and leukocyte-endothelial interactions: a sticky connection? Trends Immunol. **26**: 561–564.
16) Hoshino, A., Fujioka, K., Oku, T., Nakamura, S., Suga, M., et al. 2004. Quantum dots targeted to the assigned organelle in living cells. Microbiol. Immunol. **48**: 985–994.
17) Hoshino, A., Fujioka, K., Oku, T., Suga, M., Sasaki, Y.F., et al. 2004. Physicochemical properties and cellular toxicity of nanocrystal quantum dots depend on their surface modification. Nano Lett. **4**: 2163–2169.
18) Hoshino, A., Nagao, T., Nakasuga, A., Ishida-Okawara, A., Suzuki, K., et al. 2007. Nanocrystal quantum dot-conjugated anti-myeloperoxidase antibody as the detector of activated neutrophils. IEEE Transactions on NanoBioscience, in press.
19) Ichimori, K., Fukuyama, N., Nakazawa, H., Aratani, Y., Koyama, H., et al. 2003. Myeloperoxidase has directly-opposed effects on nitration reaction—study on myeloperoxidase-deficient patient and myeloperoxidase-knockout mice. Free Radic. Res. **37**: 481–489.
20) Ishida-Okawara, A., Ito-Ihara, T., Muso, E., Ono, T., Saiga, K., et al. 2004. Neutrophil contribution to the crescentic glomerulonephritis in SCG/Kj mice. Nephrol. Dial. Transplant. **19**: 1708–1715.
21) Ishida-Okawara, A., Nagi-Miura, N., Oharaseki, T., Takahashi, K., Okumra, A., et al. 2007. Neutrophil activation and arteritis induced by *C. albicans* water-soluble mannoprotein-beta-glucan complex (CAWS). Exp. Mol. Pathol. In press.
22) Ishida-Okawara, A., Oharaseki, T., Takahashi, K., Hashimoto, Y., Aratani, Y., et al. 2001. Contribution of myeloperoxidase to coronary artery vasculitis associated with MPO-ANCA production. Inflammation **25**: 381–387.
23) Jennette, J.C., Falk, R.J., Andrassy, K., Bacon, P.A., Churg, J., et al. 1994. Nomenclature of systemic vasculitides. Proposal of an international consensus conference. Arthritis Rheum. **37**: 187–192.
24) Kawai, Y., Okawara, A.I., Okuyama, H., Kura, F., and Suzuki, K. 2000. Modulation of chemotaxis, O(2)(−) production and myeloperoxidase release from human polymorphonuclear leukocytes by the ornithine-containing lipid and the serineglycine-containing lipid of *Flavobacterium*.

FEMS Immunol. Med. Microbiol. **28**: 205–209.
25) Kinjoh, K., Kyogoku, M., and Good, R.A. 1993. Genetic selection for crescent formation yields mouse strain with rapidly progressive glomerulonephritis and small vessel vasculitis. Proc. Natl. Acad. Sci. U.S.A. **90**: 3413–3417.
26) Klebanoff, S.J., and Coombs, R.W. 1992. Viricidal effect of polymorphonuclear leukocytes on human immunodeficiency virus-1. Role of the myeloperoxidase system. J. Clin. Invest. **89**: 2014–2017.
27) Kolls, J.K., and Linden, A. 2004. Interleukin-17 family members and inflammation. Immunity **21**: 467–476.
28) Kurihara, K., Miura, N.N., Uchiyama, M., Ohno, N., Adachi, Y., et al. 2000. Measurement of blood clearance time by Limulus G test of Candida-water soluble polysaccharide fraction, CAWS, in mice. FEMS Immunol. Med. Microbiol. **29**: 69–76.
29) Kurihara, K., Shingo, Y., Miura, N.N., Horie, S., Usui, Y., et al. 2003. Effect of CAWS, a mannoprotein-beta-glucan complex of *Candida albicans*, on leukocyte, endothelial cell, and platelet functions *in vitro*. Biol. Pharm. Bull. **26**: 233–240.
30) Lesavre, P., Noel, L.H., Gayno, S., Nusbaum, P., Reumaux, D., et al. 1993. Atypical autoantigen targets of perinuclear antineutrophil cytoplasm antibodies (P-ANCA): specificity and clinical associations. J. Autoimmun. **6**: 185–195.
31) Little, M.A., Smyth, C.L., Yadav, R., Ambrose, L., Cook, H.T., et al. 2005. Antineutrophil cytoplasm antibodies directed against myeloperoxidase augment leukocyte-microvascular interactions *in vivo*. Blood **106**: 2050–2058.
32) Moguilevsky, N., Steens, M., Thiriart, C., Prieels, J.P., Thiry, L., and Bollen, A. 1992. Lethal oxidative damage to human immunodeficiency virus by human recombinant myeloperoxidase. FEBS Lett. **302**: 209–212.
33) Morita, T., Yamamoto, T., and Churg, J. 1998. Mesangiolysis: an update. Am. J. Kidney Dis. **31**: 559–573.
34) Muso, E., Ito-Ihara, T., Ono, T., Imai, E., Yamagata, K., et al. 2004. Intravenous immunoglobulin (IVIg) therapy in MPO-ANCA related polyangiitis with rapidly progressive glomerulonephritis in Japan. Jpn. J. Infect. Dis. **57**: S17–S18.
35) Nagao, T., Matsumura, M., Mabuchi, A., Ishida-Okawara, A., Koshio, O., et al. 2007. Up-regulation of adhesion molecule expression in glomerular endothelial cells by anti-myeloperoxidase antibody. Nephrol. Dial. Transplant. **22**: 77–87.
36) Nagi-Miura, N., Shingo, Y., Adachi, Y., Ishida-Okawara, A., Oharaseki, T., et al. 2004. Induction of coronary arteritis with administration of CAWS (*Candida albicans* water-soluble fraction) depending on mouse strains. Immunopharmacol. Immunotoxicol. **26**: 527–543.
37) Neumann, I., Birck, R., Newman, M., Schnulle, P., Kriz, W., et al. 2003. SCG/Kinjoh mice: a model of ANCA-associated crescentic glomerulonephritis with immune deposits. Kidney Int. **64**: 140–148.
38) Ohno, N. 2004. Murine model of Kawasaki disease induced by mannoprotein-beta-glucan complex, CAWS, obtained from *Candida albicans*. Jpn. J. Infect. Dis. **57**: S9–S10.
39) Ornberg, R.L., Harper, T.F., and Liu, H. 2005. Western blot analysis with quantum dot fluorescence technology: a sensitive and quantitative method for multiplexed proteomics. Nat. Methods **2**: 79–81.
40) Radford, D.J., Lord, J.M., and Savage, C.O. 1999. The activation of the neutrophil respiratory burst by anti-neutrophil cytoplasm autoantibody (ANCA) from patients with systemic vasculitis requires tyrosine kinases and protein kinase C activation. Clin. Exp. Immunol. **118**: 171–179.
41) Radford, D.J., Savage, C.O., and Nash, G.B. 2000. Treatment of rolling neutrophils with antineutrophil cytoplasmic antibodies causes conversion to firm integrin-mediated adhesion. Arthritis Rheum. **43**: 1337–1345.
42) Rarok, A.A., Limburg, P.C., and Kallenberg, C.G. 2003. Neutrophil-activating potential of antineutrophil cytoplasm autoantibodies. J. Leukoc. Biol. **74**: 3–15.
43) Savage, C.O., Pottinger, B.E., Gaskin, G., Pusey, C.D., and Pearson, J.D. 1992. Autoantibodies developing to myeloperoxidase and proteinase 3 in systemic vasculitis stimulate neutrophil cytotoxicity toward cultured endothelial cells. Am. J. Pathol. **141**: 335–342.
44) Schreiber, A., Busjahn, A., Luft, F.C., and Kettritz, R. 2003. Membrane expression of proteinase 3 is genetically determined. J. Am. Soc. Nephrol. **14**: 68–75.
45) Schreiber, A., Luft, F.C., and Kettritz, R. 2004. Membrane proteinase 3 expression and ANCA-induced neutrophil activation. Kidney Int. **65**: 2172–2183.
46) Schreiber, A., Otto, B., Ju, X., Zenke, M., Goebel, U., et al. 2005. Membrane proteinase 3 expression in patients with Wegener's granulomatosis and in human hematopoietic stem cell-derived neutrophils. J. Am. Soc. Nephrol. **16**: 2216–2224.
47) Suzuki, K. 2003. Neutrophil functions of patients with MPO-ANCA-related vasculitis. Intern. Med. **42**: 552–553.
48) Suzuki, K., Muso, E., and Nauseef, W.M. 2004. Contribution of peroxidases in host-defense, diseases and cellular functions. Jpn. J. Infect. Dis. **57**: S1–S2.
49) Suzuki, K., and Okazaki, T. 2004. Contribution of myeloperoxidase in vasculitis development. Jpn. J. Infect. Dis. **57**: S2–S3.
50) van der Geld, Y.M., Oost-Kort, W., Limburg, P.C., Specks, U., and Kallenberg, C.G. 2000. Recombinant proteinase 3 produced in different expression systems: recognition by anti-PR3 antibodies. J. Immunol. Methods **244**: 117–131.
51) Voura, E.B., Jaiswal, J.K., Mattoussi, H., and Simon, S.M. 2004. Tracking metastatic tumor cell extravasation with quantum dot nanocrystals and fluorescence emission-scanning microscopy. Nat. Med. **10**: 993–998.
52) Wu, X., Liu, H., Liu, J., Haley, K.N., Treadway, J.A., et al. 2003. Immunofluorescent labeling of cancer marker Her2 and other cellular targets with semiconductor quantum dots. Nat. Biotechnol. **21**: 41–46.
53) Xiao, H., Heeringa, P., Hu, P., Liu, Z., Zhao, M., et al. 2002. Antineutrophil cytoplasmic autoantibodies specific for myeloperoxidase cause glomerulonephritis and vasculitis in mice. J. Clin. Invest. **110**: 955–963.

Available online at www.sciencedirect.com
ScienceDirect
J. of Supercritical Fluids 41 (2007) 279–284
THE JOURNAL OF Supercritical Fluids
www.elsevier.com/locate/supflu

Evidence for the production of fluorescent pyrazine derivatives using supercritical water

Yasuhiro Futamura[a,b], Kazuyuki Yahara[c], Kenji Yamamoto[a,*]

[a] *International Clinical Research Center, Research Institute, International Medical Center of Japan, 1-21-1 Toyama, Shinjuku-ku, Tokyo 162-8655, Japan*
[b] *Department of Bioactive Molecules, The National Institute of Infectious Diseases, 1-23-1 Toyama, Shinjuku-ku, Tokyo 162-8640, Japan*
[c] *Material Design Group, Material Technology Center, R & D Institute, High Performance Plastics Company, Sekisui Chemical Co., Ltd., 2-1 Hyakuyama, Shimamoto-cho, Mishima-gun, Osaka 618-8589, Japan*

Received 16 June 2006; received in revised form 12 October 2006; accepted 22 October 2006

Abstract

Potential for organic synthesis in supercritical water (SCW) was proposed in the 1990's. Here we describe the hydrothermal synthesis of low molecular fluorescent organic molecules derived from an amino acid, glycine, using an SCW flow reactor with rapid expansion cooling. Glycine aqueous solution was treated in SCW and then was poured out into the atmosphere through a narrow orifice of the needle valve to be depressurized. The product mixture solution had emission from blue to ultraviolet. HPLC fractions of the products also had fluorescence and included $C_5H_6N_2O$ and its methyl derivative. Theoretical calculation of fluorescence and absorption spectra of the candidate compounds also shows that the most probable compounds are 5- or 6-methylpyrazin-2-one and their 3-methyl derivatives. The fluorescent compounds suggest carbon-carbon bond formation as well as dehydration condensation in SCW.

Keywords: Supercritical water; Dehydration; Amino acid; Fluorescence; Pyrazinone; INDO/S

1. Introduction

Supercritical water (SCW) has received attention as a medium for chemical reactions. It not only provides advantages from the viewpoints of ecology, economics, and safety, but it is also of particular interest on its solvent parameters, for example, density, ionic product and dielectric constant [1,2]. SCW oxidation is used for organic waste disposal system [3]. It is proposed that hydrothermal condition can be applied for "SCW-catalyzed" organic chemical reaction, for example, not only hydrolysis or oxidative decomposition, but also synthesis such as addition, rearrangement and dehydration condensation. Diels–Alder reaction is the first organic synthesis study using SCW without any catalysts [4]. Ikushima and his colleagues also demonstrated the Beckmann rearrangement of cyclohexanone oxime into ε-caprolactam, the pinacol/pinacolone rearrangement and Heck coupling in SCW [5–10]. Oligopeptides are synthesized by dehydration condensation of an amino acid using subcritical water [11–13]. We recently reported longer peptide synthesis (up to 10mer) via dehydration condensation reaction using a hydrothermal flow reactor at 10 MPa and 270 °C with adiabatic expansion cooling [14]. Under higher pressure and temperature condition above the critical point of water (T_c = 374.2 °C, P_c = 22.1 MPa), herein we report synthesis of organic fluorescent compounds from an amino acid, glycine **1**. In molecular biology, fluorescent compounds such as proteins and organics are conjugated with the target molecules to observe their kinetics or dynamics, while the larger compounds sometimes change the property of the targets because of the size of conjugates. Smaller fluorescent compounds would be more useful for small targets in molecular biology.

2. Experimental

2.1. Hydrothermal reaction with adiabatic expansion cooling

Glycine and ethylenediamine-*N,N,N′,N′*-tetraacetic acid (EDTA) was purchased from Wako Pure Chemical Industries,

* Corresponding author. Tel.: +81 3 3202 7181; fax: +81 3 3202 7364.
E-mail address: backen@ri.imcj.go.jp (K. Yamamoto).

0896-8446/$ – see front matter © 2006 Elsevier B.V. All rights reserved.
doi:10.1016/j.supflu.2006.10.008

Ltd. (Osaka, Japan) and Dojindo Laboratories (Kumamoto, Japan), respectively. The concentration of glycine aqueous solution was 1 mol L^{-1} without pH control. Using a hydrothermal flow reactor with adiabatic expansion cooling (AKICO, Tokyo, Japan) [14], the glycine solution was incubated at 400 °C and 25 MPa for about 1 min when the flow rate was 10 mL min^{-1}. At the end of the flow reactor, the solution was quenched and depressurized from the needle valve with the adiabatic expansion method.

2.2. Analytical methods

The photoluminescent properties were determined with a fluorescence spectrophotometer FP-6500 (JASCO Co., Hachioji, Tokyo, Japan).

Reversed phase-high performance liquid chromatography (HPLC) was performed with a 600E or 600 System Controller (Waters), a 2487 Dual Wavelength Absorbance Detector (Waters) or a 996 Photodiode Array (PDA) Detector (Waters) for absorbance detection, and a 2475 Multi Wavelength / Scanning Fluorescence Detector (Waters). Column, Waters Xterra MS C_{18} 2.5 μm (ϕ = 4.6 mm; column length, 50 mm); mobile phase, 10 mmol mL^{-1} trifluoroacetic acid (TFA); flow rate, 0.5 ml min^{-1}. Before injection of the reaction solution into the HPLC system, the sample was filtrated by a 0.22 μm centrifugal filter device (Millipore Ultrafree-MC). LC-TOF-MS was performed using a Waters/Micromass Quattro Premier (Nihon Waters K.K., Tokyo, Japan). Supported by Toray Research Center, Inc. (Kamakura, Japan), LC-NMR was measured at 25 °C in 10 mmol mL^{-1} of TFA/D_2O in the stop flow mode using a 600 MHz spectrometer (Varian Unity Inova600, CA, USA).

2.3. Theoretical calculations

Theoretical spectra of absorbance and fluorescence were calculated as follows. Structure optimization of ground and excited states was performed using Gaussian 98 or Gaussian 03 for Windows (Gaussian Inc., Wallingford, Connecticut, USA) based on density-functional-theory at the B3LYP/6-31 + G(d,p) level. Excited state was calculated by configuration interaction-singles (CIS) method. Theoretical UV absorption and fluorescence spectra were calculated by a semi-empirical molecular orbital method, intermediate neglect of diatomic differential overlap/spectroscopy (INDO/S) using MOS-F in WinMOPAC package (Fujitsu, Ltd., Kawasaki, Japan).

3. Results

We injected glycine aqueous solution of 1 mol L^{-1} into a hydrothermal flow reactor with adiabatic expansion cooling made of stainless steel, SUS316 [14]. The glycine solution was incubated at 400 °C and 25 MPa for about 1 min when the flow rate was 10 mL min^{-1}. After heating and pressurizing the glycine solution, it was quenched and depressurized through the needle valve with the gap area of less than 10 mm^2.

The droplets through the needle valve at the end of the hydrothermal reactor had a strong fluorescence with blue-light

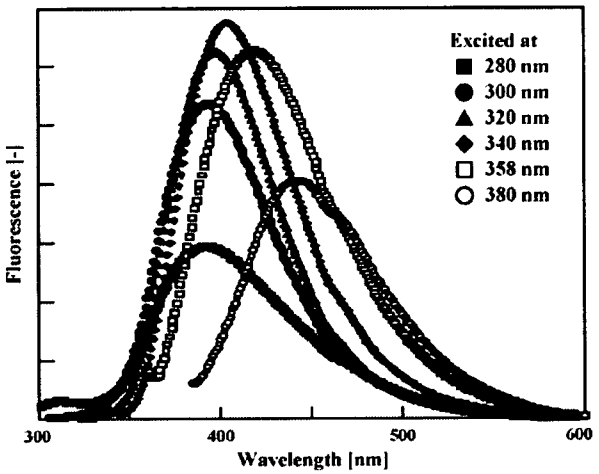

Fig. 1. Emission spectra of the crude hydrothermal products from glycine aqueous solution. Excitation wavelength is changed between 280 to 380 nm.

emission. Fig. 1 shows the emission spectra of the crude droplets excited with ultraviolet (UV) light at various wavelengths. The wavelength of the maximum fluorescence (λ_{max}) is 410 nm when the solution is excited at 330 nm. The overlay of the emission spectra shows a peak at about 390 nm. Even with addition of excessive EDTA as a metal ion chelator, the fluorescence never vanished (data not shown).

We performed reversed-phase HPLC with UV absorption and fluorescence detection systems. As shown in Fig. 2, some peaks were detected by fluorescence, and the major two peaks were designated as LC peaks 2 and 4, respectively. The maximum wavelengths of UV absorption of both peaks were observed at 329 nm by LC-PDA (Table 1). The UV absorption and fluorescence spectroscopy suggest that the compounds have π-electron conjugated systems, such as aromatic rings.

Then we measured the accurate masses of the molecules in each peak using LC-MS in both positive and negative ion modes

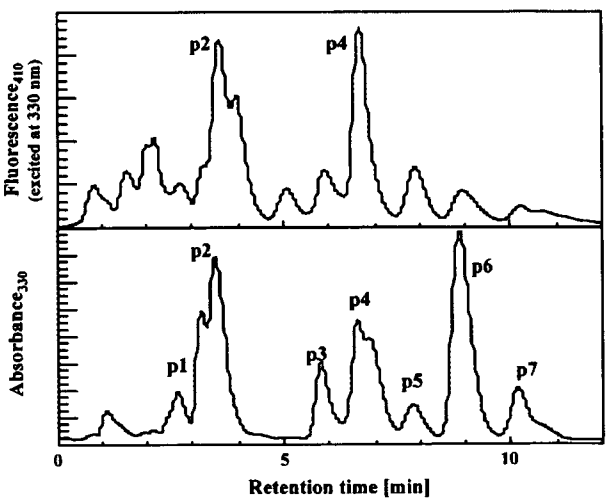

Fig. 2. Chromatogram of the crude hydrothermal products from glycine aqueous solution detected by fluorescence at 410 nm excited at 330 nm (upper) and absorbance at 330 nm (lower).

Table 1
Maximum wavelength of absorption and emission of the hydrothermal products (experimental) and their candidates (theoretical)

	λ_{max} (nm)	
	LC/PDA	Spectrofluorometry
Experimental		
LC peak 2 ($C_5H_6N_2O$)	329	390–410
LC peak 4 ($C_6H_8N_2O$)	329	

		λ_{max} (nm)	
	CAS number	Absorption	Emission
Theoretical			
$C_4H_2N_2O_2$			
pyrazine-2,5-dione	[88982-21-2]	330	–
$C_5H_6N_2O$			
N^1-methylpyrazin-2-one	[3149-27-7]	334	380
3-methylpyrazin-2-one (keto form)	[19838-07-4]	328	395
3-methylpyrazin-2-ol (enol form)	Not registered	328	285
5-methylpyrazin-2-one (keto form)	[20721-17-9]	343	403
5-methylpyrazin-2-ol (enol form)	Not registered	330	277
6-methylpyrazin-2-one (keto form)	[20721-18-0]	337	392
6-methylpyrazin-2-ol (enol form)	Not registered	329	285
pyrazinemethanol	[6705-33-5]	282	270
2-methylpyrazine-1-oxide	[31396-35-7]	293	306
2-methylpyrazine-4-oxide	[25594-37-0]	305	311
5-hydroxy-4-methylpyrimidine	[35231-56-2]	312	–
2-hydroxy-4-methylpyrimidine (keto form)	[41398-85-0]	316	344
2-hydroxy-5-methylpyrimidine (keto form)	[42839-09-8]	322	366
2-methoxypyrazine	[65150-77-8]	332	335
3-hydroxy-N^1-methylpyridazine	[73619-53-1]	331	445
5-hydroxy-2-methylpyrimidine	[17358-44-1]	322	311
$C_6H_8N_2O$			
3,5-dimethylpyrazin-2-one (keto form)	[60187-00-0]	334	321
3,6-dimethylpyrazin-2-one (keto form)	[16289-18-2]	333	320
5,6-dimethylpyrazin-2-one (keto form)	[57229-36-4]	346	392

by electrospray ionization (ESI). After the LC separation using TFA as a mobile phase, no signals were detected with MS scan in negative ion mode. LC-TOF-MS data in positive ion mode show that the protonated masses of major molecules ($[M+H]^+$) at 4.602 min (LC peak 2) and 7.572 min (LC peak 4) are *m/z* 111.0550 and *m/z* 125.0724, respectively, suggesting that the molecular formulae of $[M+H]^+$ are $C_5H_7N_2O$ (theoretical mass is 111.0558 amu) and $C_6H_9N_2O$ (125.0715 amu), respectively (Fig. 3).

The mass gap between the two products is 14.0174 amu, corresponding to methylene group $-CH_2-$ (theoretical mass of $-CH_2-$ is 14.0157 amu). Concerning the degree of unsaturation of $C_5H_6N_2O$ and $C_6H_8N_2O$, the index of hydrogen deficiency (IHD) of $C_xH_yN_zO_w$ is represented as $x-y/2+z/2+1$, where x, y, z and w are the numbers of carbon, hydrogen, nitrogen and oxygen, respectively. The IHDs of $C_5H_6N_2O$ and $C_6H_8N_2O$ are four, suggesting that they have four multiple bonds or rings.

As for the hydrothermal reaction from glycine to the $C_5H_6N_2O$ and $C_6H_8N_2O$, we have previously reported dehydration oligomerization of glycine under the milder hydrothermal condition to produce diglycine **2** and so on, and also observed great amount of diketopiperazine **3** [14]. It was reported that **2** is easily cyclized by dehydration to produce **3** in SCW [12]. There-

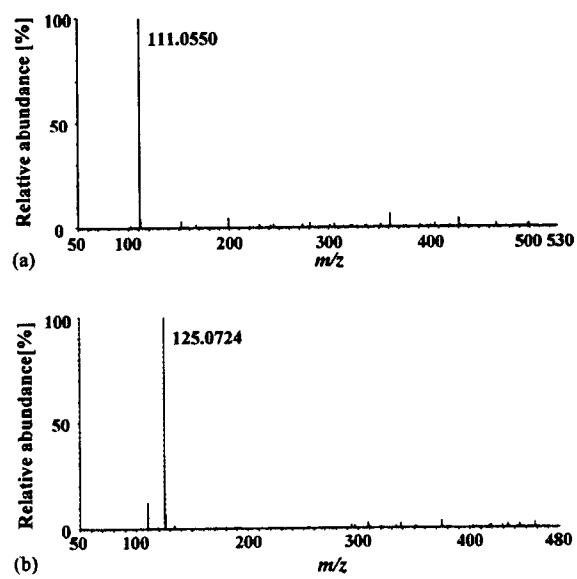

Fig. 3. Mass spectra of (a) LC peak 2 and (b) LC peak 4 in positive ion mode using Waters/Micromass Quattro Premier.

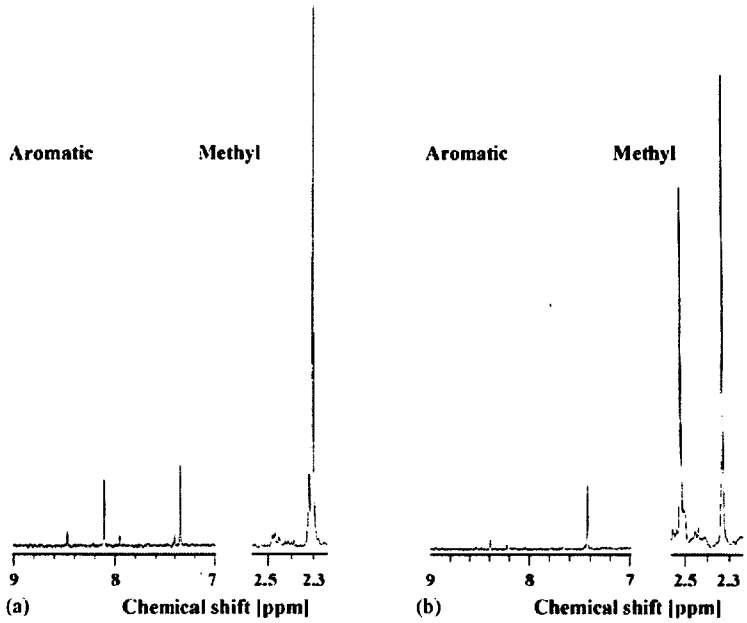

Fig. 4. Aromatic and methyl regions of ^{1}H NMR spectra of (a) LC peak 2 and (b) peak 4. ^{1}H NMR measurement was performed in 10 mmol mL^{-1} TFA in D_2O at 25 °C.

fore, in the reaction that we performed under higher pressure and temperature condition, **2** and **3** would be also synthesized. The difference of the molecular formula between **3** and $C_5H_6N_2O$ is one carbon atom added and one oxygen atom reduced. If we assume more dehydration ($-H_2O$) under the hydrothermal conditions, addition of methylene group ($+CH_2$) is consistent with the formation of $C_5H_6N_2O$. We speculate that more dehydration and methylation of **3** make methylpyrazinone and dimethylpyrazinone, of which molecular formulae are $C_5H_6N_2O$ and $C_6H_8N_2O$, respectively.

Then we performed LC-NMR in the stop-flow mode. The NMR spectrum of each fraction shows much more proton peaks than those of theoretical formula introduced by accurate mass, suggesting insufficient LC separation. On the other hand, the LC peak 2 ($C_5H_6N_2O$) includes two singlet signals at the chemical shift of 7.357 and 8.116 ppm, suggesting two aromatic protons without or with a weak ^{1}H–^{1}H spin–spin coupling (Fig. 4a). The existence of aromatic signals is consistent with the assumption that the compound of $C_5H_6N_2O$ is a methylpyrazinone. Judging from the ^{1}H NMR of pyrazinone [15], the singlet signal at 8.116 ppm would be derived from the proton at position 3. Furthermore, the two aromatic signals do not have a strong ^{1}H–^{1}H spin–spin coupling. Therefore, the most probable compound would be 5-methylpyrazin-2-one **4a**, or 6-methylpyrazin-2-one **4b**, of which protons are not adjacent to each other on the aromatic ring. In the LC peak 4 ($C_6H_8N_2O$), on the other hand, only a singlet signal derived from the aromatic proton was observed and the other singlet signal around 8.1 ppm disappeared. Instead, a methyl proton signal appeared at 2.506 ppm in addition to at 2.323 ppm (Fig. 4b). It was explained by the substitution of the aromatic proton at position 3 of $C_5H_6N_2O$ for a methyl group.

Although more than 200 compounds of $C_5H_6N_2O$ are registered in the CAS database, not all the compounds have fluorescence. To confirm that the fluorescent compounds were the pyrazinone derivatives, we calculated theoretical UV absorption and fluorescence spectra of various heterocyclic compounds of which molecular formulae are registered as $C_5H_6N_2O$ and $C_6H_8N_2O$ in the CAS database (Table 1) by a semi-empirical molecular orbital method, intermediate neglect of diatomic differential overlap/spectroscopy (INDO/S). Among the $C_5H_6N_2O$ compounds, N^1-methylpyrazin-2-one, 3-methylpyrazin-2-one, 5-methylpyrazin-2-one and 6-methylpyrazin-2-one are consistent with the experimental spectra of UV absorption and fluorescence, although the other compounds have neither a strong absorption between 310 and 350 nm nor a strong fluorescence between 370 and 430 nm.

4. Discussion

After hydrothermal treatment of glycine aqueous solution with SCW, the solution showed blue emission under UV light. The absorption and photoluminescent properties of the product suggest π-electron conjugated systems such as an aromatic ring. From the LC-MS analyses, quite simple compounds were included in the fluorescent fractions of HPLC. The accurate masses of protonated ions suggest that the fluorescent compounds are $C_5H_6N_2O$ and $C_6H_8N_2O$. The LC-NMR analyses indicate that the compound in the LC peak 2 has two aromatic protons and a methyl group, and the compound in the LC peak 4 has an aromatic proton and two methyl groups. The MS and ^{1}H NMR data suggest that the two fluorescent compounds are methyl and dimethyl derivatives of pyrazin-2-one. From the theoretical calculations of ground state and excited state of var-

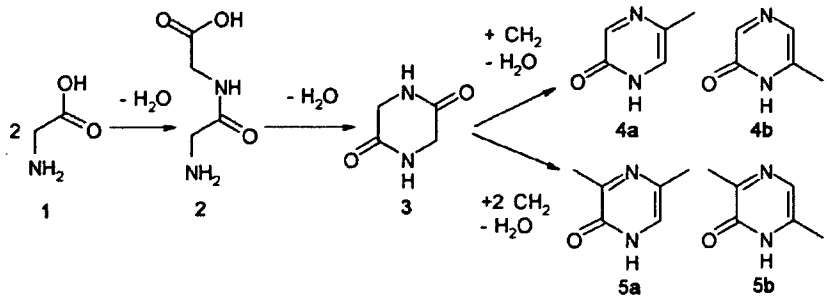

Scheme 1. Possible synthetic pathway of fluorescent substance under hydrothermal condition.

ious $C_5H_6N_2O$ compounds, the absorption and fluorescence spectra of N^1-methylpyrazin-2-one, 3-methylpyrazin-2-one, 5-methylpyrazin-2-one and 6-methylpyrazin-2-one are consistent with the experimental spectra. The ^{1}H NMR spectrum of the LC peak 2, however, indicates that N^1-methylpyrazin-2-one, which has three aromatic protons at the positions 3, 5 and 6, could be eliminated from the candidates. 3-methylpyrazin-2-one, which has two aromatic protons adjacent to each other at the positions 5 and 6 which should have a strong vicinal ^{1}H–^{1}H spin–spin coupling ($^3J_{5,6} \sim 4$ Hz) [15], also could be eliminated from the candidates, because two singlet signals derived from the aromatic protons were detected in the LC peak 2 by LC-NMR analyses. Therefore, the fluorescence compounds synthesized from glycine in SCW is thought to be 5-methylpyrazin-2-one **4a**, or 6-methylpyrazin-2-one **4b**. Judging from the comparison between the ^{1}H NMR spectra of the LC peaks 2 and 4 shows that the $C_6H_8N_2O$ compound is 3-methyl derivative of $C_5H_6N_2O$. Theoretical absorption spectra of 3,5-dimethylpyrazin-2-one **5a** and 3,6-dimethylpyrazin-2-one **5b** are also compatible with the experimental data of LC peak 4. On the other hand, fluorescent alkyl pyrazinones (flavacol, deoxyaspergillic acid and so on) have been reported to show the absorption and fluorescent spectra that are quite similar to our experimental data [16].

Concerning the integral values of ^{1}H NMR, the ratios of methyl protons at 2.506 and 2.323 ppm in LC peak 4 were 5.2 and 6.0, respectively, when normalized by the aromatic proton signal at 7.447 ppm. In LC peak 2, the ratio of the methyl proton at 2.302 ppm to the aromatic proton was 8.9. However, based on our proposal structures, the ratios of the methyl to the aromatic protons were expected to be 3. This discrepancy might be explained by the proton-deuterium exchange in the D_2O solvent at low pD during the stopped-flow NMR measurement, which caused the decrease of the signals of aromatic protons. On the heterocyclic aromatic rings, C-H protons, especially ones adjacent to nitrogen atoms, are known to be easy to exchange for the deuterium in the solvent [17–20].

To obtain oligoglycines, we previously reported subcritical water treatment of glycine at 10 MPa and 270 °C, but the products had little fluorescence when excited with UV light [14]. On the contrary, under higher pressure and temperature conditions, it was possible that glycine decomposed into such compounds as ammonia, carbon dioxide, methylamine, formic acid, acetic acid and glycolic acid, which was inferred in Sato's study [21]. Carbon–carbon bond formation should be essential to produce pyrazinone methyl derivatives from glycine in SCW. Morooka et al. reported that C–C bond was formed in SCW from aldehydes [22–24]. Sato et al. have also reported alkylation of phenol with formyl compounds in SCW [25]. This report suggests that formaldehyde may be a source of methyl group in SCW. Therefore, such a formyl compound would be a methyl donor for C–C bond formation in our case.

The yields of LC peaks 2 and 4 can be estimated to be 0.5 or 1% each, judging from the absorbance at 330 nm, on the assumption that the molar extinction coefficient is about 10^4 L mol^{-1} cm^{-1} [26]. Even though the yields are low, the fluorescence is strong. On the other hand, organic fluorescent molecules, such as *Aequorea* Green Fluorescent Protein (GFP; molecular weight, 27 kDa) and fluorescein isothiocyanate (FITC; molecular weight, 389), are widely used for probes, which are fused with other proteins or are conjugated with RNA and DNA. The methylpyrazinone is one third smaller than FITC and should be useful as a probe, when it is conjugated with much smaller biological molecules such as metabolites, drugs and so on.

5. Conclusions

Herein, we report synthesis of fluorescent compounds from glycine by treatment with SCW. Chemical analyses and theoretical calculation suggest production of methyl- and dimethylpyrazin-2-ones in SCW (Scheme 1).

Acknowledgements

We thank Mr. Tomomasa Goto from Department of Chemical System Engineering, Graduate School of Engineering, the University of Tokyo, Japan, for hydrothermal experiments, Drs. Etsuko Suzuki and Michiko Kanai of Nihon Waters K.K. (Tokyo, Japan) for LC-MS analyses, as well as Dr. Ken Kawaguchi of Toray Research Center, Inc. (Kamakura, Japan) for LC-NMR analyses.We also thank Mr. Kazuyuki Itou for the preparation of the manuscript. This work was partly supported by the research grants for Learning from Nature for Production 2002–2003 from Sekisui Chemical Co., Ltd., and by Grants-in-Aid for Scientific Research from the Ministry of Health, Labor and Welfare, Japan.

References

[1] K. Omata, Y. Futamura, K. Yamamoto, Supercritical fluids studied by Monte Carlo simulations, Adv. Sci. Technol. 42 (2004) 413–420.

[2] D. Bröll, C. Kaul, A. Krämer, P. Krammer, T. Richter, M. Jung, H. Vogel, P. Zehner, Chemistry in supercritical water, Angew. Chem. Int. Ed. 38 (1999) 2998–3014.

[3] S. Yesodharan, Supercritical water oxidation: An environmentally safe method for the disposal of organic wastes, Curr. Sci. 82 (2002) 1112–1122.

[4] M.B. Korzenski, J.W. Koils, Diels-Alder reactions using supercritical water as an aqueous solvent medium, Tetrahedr. Lett. 38 (1997) 5611–5614.

[5] O. Sato, Y. Ikushima, T. Yokoyama, Noncatalytic Beckmann rearrangement of cyclohexanone-oxime in supercritical water, J. Org. Chem. 63 (1998) 9100–9102.

[6] Y. Ikushima, O. Sato, M. Hatakeda, T. Yokoyama, M. Arai, Noncatalytic organic synthesis using supercritical water: the peculiarity near the critical point, Angew. Chem. Int. Ed. 38 (1999) 2910–2914.

[7] Y. Ikushima, O. Sato, M. Hatakeda, T. Yokoyama, M. Arai, Acceleration of synthetic organic reactions using supercritical water: noncatalytic Beckmann and pinacol rearrangements, J. Am. Chem. Soc. 122 (2000) 1908–1918.

[8] Y. Ikushima, O. Sato, M. Sato, K. Hatakeda, M. Arai, Innovations in chemical reaction processes using supercritical water: an environmental application to the production of ε-caprolactam, Chem. Eng. Sci. 58 (2003) 935–941.

[9] R. Zhang, F. Zhao, M. Sato, Y. Ikushima, Noncatalytic Heck coupling reaction using supercritical water, Chem. Commun. 2003 (2003) 1548–1549.

[10] R. Zhang, O. Sato, F. Zhao, M. Sato, Y. Ikushima, Heck coupling reaction of iodobenzene and styrene using supercritical water in the absence of a catalyst, Chemistry 10 (2004) 1501–1506.

[11] E. Imai, H. Honda, K. Hatori, A. Brack, K. Matsuno, Elongation of oligopeptides in a simulated submarine hydrothermal system, Science 283 (1999) 831–833.

[12] D.K. Alargov, S. Deguchi, K. Tsujii, K. Horikoshi, Reaction behaviors of glycine under super- and subcritical water conditions, Origins Life Evol. Biosphere 32 (2002) 1–12.

[13] M.N. Islam, T. Kaneko, K. Kobayashi, Reaction of amino acids in a supercritical water-flow reactor simulating submarine hydrothermal systems, Bull. Chem. Soc. Jpn. 76 (2003) 1171–1178.

[14] T. Goto, Y. Futamura, Y. Yamaguchi, K. Yamamoto, Condensation reactions of amino acids under hydrothermal conditions with adiabatic expansion cooling, J. Chem. Eng. Jpn. 38 (2005) 295–299.

[15] R.H. Cox, A.A. Bothner-By, Proton nuclear magnetic resonance spectra of monosubstituted pyrazines, J. Phys. Chem. 72 (1968) 1646–1649.

[16] T. Yokotsuka, M. Sasaki, T. Kikuchi, Y. Asao, A. Nobuhara, Studies in the compounds produced by moulds. Part I. Fluorescent compounds produced by Japanese industrial moulds, Nippon Nogei Kagaku Zasshi 41 (1967) 32–38.

[17] R.S. Norton, J.H. Bradbury, Kinetics of hydrogen-deuterium exchange of tryptophan and tryptophan peptides in deutero-trifluoroacetic acid using proton magnetic resonance spectroscopy, Mol. Cell. Biochem. 12 (1976) 103–111.

[18] J.H. Bradbury, B.E. Chapman, F.A. Pellegrino, Hydrogen-deuterium exchange kinetics of the C-2 protons of imidazole and histidine compounds, J. Am. Chem. Soc. 95 (1973) 6139–6140.

[19] I. Kim, S. Watanabe, Y. Muto, K. Hosono, K. Takai, H. Takaku, G. Kawai, K. Watanabe, S. Yokoyama, Selective deuteration of RNA for NMR signal assignment, in: Nucleic Acids Symposium Series, 34, 1995, pp. 123–124.

[20] R. Brandes, A. Ehrenberg, Kinetics of the proton-deuteron exchange at position H8 of adenine and guanine in DNA, Nucl. Acids Res. 14 (1986) 9491–9508.

[21] N. Sato, H. Daimon, K. Fujie, Decomposition of glycine in high temperature and high pressure water, Kagaku Kogaku Ronbunshu 28 (2002) 113–118.

[22] S. Morooka, C. Wakai, N. Matubayasi, M. Nakahara, Acid-catalyzed hydrothermal formation of carbon-carbon bond in glycolic acid from a series of formaldehyde producers, Chem. Lett. 33 (2004) 624–625.

[23] Y. Nagai, S. Morooka, N. Matubayasi, M. Nakahara, Mechanisms and kinetics of acetaldehyde reaction in supercritical water: noncatalytic disproportionation, condensation, and decarbonylation, J. Phys. Chem. A 108 (2004) 11635–11643.

[24] S. Morooka, C. Wakai, N. Matubayasi, M. Nakahara, Hydrothermal carbon–carbon bond formation and disproportionations of C1 aldehydes: formaldehyde and formic acid, J. Phys. Chem. A 109 (2005) 6610–6619.

[25] T. Sato, G. Sekiguchi, T. Adschiri, K. Arai, Alkylation of phenol with carbonyl compounds in supercritical water, J. Chem. Eng. Jpn. 36 (2003) 339–342.

[26] G.T. Newbold, F.S. Spring, Pyrazine derivatives. Part II. A synthesis of a racemic 2-hydroxy-3:6-di-sec.-butylpyrazine and its relationship to deoxyaspergillic acid, J. Chem. Soc. 1947 (1947) 373–378.

Inhibition of CCL1-CCR8 Interaction Prevents Aggregation of Macrophages and Development of Peritoneal Adhesions[1]

Akiyoshi Hoshino,* Yuki I. Kawamura,†¶ Masato Yasuhara,§ Noriko Toyama-Sorimachi,† Kenji Yamamoto,‡ Akihiro Matsukawa,‖ Sergio A. Lira,# and Taeko Dohi[2†]

Peritoneal adhesions are a significant complication of surgery and visceral inflammation; however, the mechanism has not been fully elucidated. The aim of this study was to clarify the mechanism of peritoneal adhesions by focusing on the cell trafficking and immune system in the peritoneal cavity. We investigated the specific recruitment of peritoneal macrophages (PMϕ) and their expression of chemokine receptors in murine models of postoperative and postinflammatory peritoneal adhesions. PMϕ aggregated at the site of injured peritoneum in these murine models of peritoneal adhesions. The chemokine receptor CCR8 was up-regulated in the aggregating PMϕ when compared with naive PMϕ. The up-regulation of CCR8 was also observed in PMϕ, but not in bone marrow-derived Mϕ, treated with inflammatory stimulants including bacterial components and cytokines. Importantly, CCL1, the ligand for CCR8, a product of both PMϕ and peritoneal mesothelial cells (PMCs) following inflammatory stimulation, was a potent enhancer of CCR8 expression. Cell aggregation involving PMϕ and PMCs was induced in vitro in the presence of CCL1. CCL1 also up-regulated mRNA levels of plasminogen activator inhibitor-1 in both PMϕ and PMCs. *CCR8* gene-deficient mice or mice treated with anti-CCL1-neutralizing Ab exhibited significantly reduced postoperational peritoneal adhesion. Our study now establishes a unique autocrine activation system in PMϕ and the mechanism for recruitment of PMϕ together with PMCs via CCL1/CCR8, as immune responses of peritoneal cavity, which triggers peritoneal adhesions. *The Journal of Immunology,* 2007, 178: 5296–5304.

The serosal membrane of viscera and the peritoneal cavity are involved in numerous types of inflammation and surgical intervention. For example, in the case of surgery, postoperative adhesions occur in the majority of patients following laparotomy and laparoscopy (1, 2). Peritoneal adhesions cause significant signs and symptoms including intestinal obstruction, chronic pelvic pain and infertility, and eventually a second more serious surgery is often required. Thus, adhesions in the peritoneal cavity are both life-threatening and an enormous cost for patient care. For example, 34.6% of patients who had undergone intra-abdominal surgery were readmitted within the next 10 years for a disorder directly or possibly related to adhesions, or for abdominal or pelvic surgery that could be potentially complicated by adhesions (2). Despite the large number of surgical operations performed daily, the mechanism for peritoneal adhesions is not well-understood. Previous reports showed that peritoneal injury is triggered by leakage of plasma proteins, followed by formation of fibrinous deposits and proliferation of fibroblasts (3). A rapid and transient influx of neutrophils into the peritoneal cavity also occurs followed by an accumulation of mononuclear cells, largely macrophages (Mϕ)[3] (4, 5). CD4-positive T cells also play a significant role in peritoneal adhesions together with the T cell-derived proinflammatory cytokine, IL-17 (6), and the programmed death-1 inhibitory pathway (7). Although active roles for these cells in adhesions have been shown (8, 9), little is yet known about the cell origin or the dynamics of migration to help explain the peritoneal adhesion events. Inflammation such as appendicitis, endometriosis, and pelvic inflammatory disease can also cause peritoneal adhesion, which can lead to infertility and reproductive problems. In the case of Crohn's disease, intestinal transmural ulcerations with fissures or fistulas are the most important pathological findings (10). These Crohn's disease lesions involve the intestinal serosa and mesentery. The characteristic changes in the serosal surface, including fat wrapping, correlate directly with overall extent of inflammatory changes: the stricture of the intestine (10, 11), the depth of lymphoid aggregate penetration, and the number of lymphoid aggregates in the underlying ileal wall (12). These observations suggest that inflammation of viscera is not limited to the organ, but provokes responses in the peritoneal cavity as well. Most importantly, pathological changes in the peritoneal cavity cause serious symptoms and directly affect the quality of life of patients.

*Department of Medical Ecology and Informatics, †Department of Gastroenterology, and ‡Research Institute, International Medical Center of Japan, Tokyo, Japan; §Department of Pharmacokinetics and Pharmacodynamics, Hospital Pharmacy, Tokyo Medical and Dental University Graduate School, Tokyo, Japan; ¶G.S. Planz Company, Tokyo, Japan; ‖Department of Pathology and Experimental Medicine, Graduate School of Medical, Dentistry, and Pharmaceutical Sciences, Okayama University, Okayama, Japan; and #Immunology Center, Mount Sinai School of Medicine, New York, NY 10029

Received for publication October 17, 2006. Accepted for publication January 23, 2007.

The costs of publication of this article were defrayed in part by the payment of page charges. This article must therefore be hereby marked *advertisement* in accordance with 18 U.S.C. Section 1734 solely to indicate this fact.

[1] This work was supported in part by Medical Techniques Promotion Research Grant H14-nano-004 from the Ministry of Health, Labor, and Welfare of Japan; grants and contracts from the Ministry of Health, Labor, and Welfare; the Ministry of Education, Culture, Sports, Science, and Technology; the Japan Health Sciences Foundation; and the Japan Science and Technology Agency.

[2] Address correspondence and reprint requests to Dr. Taeko Dohi, Department of Gastroenterology, Research Institute, International Medical Center of Japan, Toyama 1-21-1, Shinjuku, Tokyo 162-8655, Japan. E-mail address: dohi@ri.imcj.go.jp

[3] Abbreviations used in this paper: Mϕ, macrophage; BMϕ, bone marrow-derived Mϕ; PMϕ, peritoneal Mϕ; QD, quantum dot; PGN, peptidoglycan; pAb, polyclonal Ab; TNBS, 2,4,6-trinitrobenzene sulfonic acid; PTX, pertussis toxin; CIMA, chemokine-induced macrophage aggregation; PMC, peritoneal mesothelial cell; tPA, tissue-type plasminogen activator; PAI-1, plasminogen activator inhibitor-1.

Table I. *List of primers for RT-PCR*

	Forward	Reverse
CCR1	GTGTTCATCATTGGAGTGGTGG	GGTTGAACAGGTAGATGCTGGTC
CCR2	TGTTACCTCAGTTCATCCACGG	CAGAATGGTAATGTGAGCAGGAAG
CCR3	TTGCAGGACTGGCAGCATT	CCATAACGAGGAGAGGAAGAGCTA
CCR4	TCTACAGCGGCATCTTCTTCAT	CAGTACGTGTGGTTGTGCTCTG
CCR5	CATCGATTATGGTATGTCAGCACC	CAGAATGGTAGTGTGAGCAGGAA
CCR6	ACTCTTTGTCCTCACCCTACCG	ATCCTGCAGCTCGTATTTCTTG
CCR7	CATCAGCATTGACCGCTACGT	GGTACGGATGATAATGAGGTAGCA
CCR8	ACGTCACGATGACCGACTACTAC	GAGACCACCTTACACATCGCAG
CCR9	CCATTCTTGTAGTGCAGGCTGTT	AAGCTTCAAGCTACCCTCTCTCC
CCR10	AGAGCTCTGTTACAAGGCTGATGTC	CAGGTGGTACTTCCTAGATTCCAGC
CXCR1	TTGCACCAACCAAGGTATCAAG	GATGAAGAAGATGCCGCTGTAG
CXCR2	CATCTTATACAACCGGAGCACC	TAGTAACCACATGGCTATGCACAC
CXCR3	ATCAGGCGCTTCAATGCCAC	TGGCTTTCTCGACCACAGTT
CXCR4	TACATCTGTGACCGCCTTTACC	TCCACTTGTGCACGATGCT
CXCR5	TCCTACTACCGATGCTTGTGATG	ACGCCAGCGAAGGTGTAAA
CCL1	GCTGCCGTGTGGATACAGGA	GAATACCACAGCTGGGGGAT
tPA	CCAGACCGAGACTTGAAGCCC	ACACCCTTTCCCAACATAGCAG
PAI-1	ATCAATGACTGGGTGGAAAG	AGCCTGGTCATGTTGCCCTT
GAPDH	AGTATGACTCCACTCACGGCAA	TCTCGCTCCTGGAAGATGGT

However, the mechanism of peritoneal inflammation has not been fully understood at the cellular and molecular levels.

In this study, we postulated that there is a common serosal defense system that responds to both visceral inflammation and surgical stress. To clarify the molecular basis for peritoneal inflammation and tissue remodeling, we used two mouse models of postoperative and postinflammatory peritoneal adhesions. These models were used to study the traffic patterns of Mϕ in the peritoneal cavity. In this study, we describe a chemokine system that is specific for peritoneal Mϕ (PMϕ) but not bone marrow-derived Mϕ (BMϕ), a system that plays a significant role in both postoperative and postinflammatory peritoneal adhesion events.

Materials and Methods

Mice

Male 6- to 7-wk-old C57BL/6J mice obtained from CLEA Japan were maintained under pathogen-free conditions in a facility in the Research Institute, International Medical Center of Japan (IMCJ). Some experiment using *CCR8* gene-deficient ($CCR8^{-/-}$) mice of C57BL/6 background were performed using mice maintained under pathogen-free conditions in the facility of Okayama University. All experiments were performed according to the Institutional Guidelines for the Care and Use of Laboratory Animals in Research and with the approval of the local ethics committee.

Materials

Fluorescent nanocrystal quantum dots (QDs) (red emission) were produced as described previously (13, 14). Recombinant mouse CCL1 and MCP1 were purchased from R&D Systems. Rat anti-mouse CCL1 mAb and a control rat IgG were purchased from R&D Systems and The Jackson Laboratory, respectively. LPS from *Escherichia coli* O55B5 and peptidoglycan (PGN) from *Staphylococcus aureus* were purchased from Sigma-Aldrich and Fluka, respectively. Phosphorothioate-stabilized CpG oligodeoxynucleotide (5′-TCCATGACGTTCCTGATGCT-3′) was purchased from Takara Bio. Recombinant mouse TNF-α and IL-1β were purchased from PeproTech. For immunohistological examination, cryosections were stained with FITC-, PE-, or biotin-labeled anti-CD11b, anti-F4/80, anti-VLA4 (CD49a), and anti-Gr-1 mAbs (BD Pharmingen), rabbit anti-CCR8 polyclonal Ab (pAb; Abcam), and rabbit anti-mouse pan-cytokeratin pAb (Santa Cruz Biotechnology) followed by Alexa Fluor streptavidin (Invitrogen Life Technologies) or FITC-labeled goat anti-rabbit IgG pAb (Southern Biotechnology Associates).

Histological analysis

Tissues were snap-frozen and 6-μm sections were prepared and stained with H&E. For immunostaining, sections were fixed with cold acetone for 10 min, dried, and treated with Blockace (Dainippon Pharmaceuticals), incubated with indicated Abs followed by secondary Abs or fluorescent labeled streptavidin described in *Materials*. Images were captured with a fluorescence microscope (BX50/BXFLA; Olympus) equipped with a CCD camera. Merged images were produced using Adobe Photoshop CS2 (Adobe Systems).

Preparation of QD-labeled Mϕ and induction of postinflammatory and postoperative peritoneal adhesions

The cells collected from the peritoneal cavity were incubated in DMEM with 2% FCS for 45 min at 37°C on plastic dishes. After removal of the nonadherent cells by two washing steps, the adherent cells were gently scraped off with a silicon rubber scraper and used as naive PMϕ. Composition of this PMϕ preparation was constantly 92.9 ± 4.3% (mean ± 1 SD of four preparations) of CD11b-positive cells (granulocytes and Mϕ) and 87.5 ± 3.6% of F4/80-positive cells (Mϕ). The BMϕ were induced by M-CSF as described previously (15, 16). In some experiments, adherent PMϕ and BMϕ were incubated with QD solutions and labeled as reported previously (14), washed, and then scraped off. The labeling efficiency was 88%, and total cells were used for all experiments. We confirmed that the preparation and labeling process of PMϕ did not cause significant alteration in the expression of chemokine receptors, surface markers, and cell viability.

A model for postoperative peritoneal adhesions was created in mice as previously described (17). Briefly, a laparotomy was performed through a midline incision and two ischemic buttons were created on both sides of the parietal peritoneum by grasping the peritoneum with a hemostat clamp and ligating the base of the segment with a 4-0 silk suture. In some experiments, the QD-labeled PMϕ were injected i.p. after closing the abdominal wall. To induce colitis-associated peritoneal adhesions, a 2% solution of 2,4,6-trinitrobenzene sulfonic acid (TNBS; Research Organics)/ethanol 1:1 by volume was given rectally (4 μl/g body weight) (18). In some experiments, QD-labeled naive PMϕ were transferred by the i.p. routes 2 h before the induction of colitis.

Laser capture microdissection

Frozen sections were prepared from the colonic tissues with colitis and then stained with the HistoGene LCM Frozen Section Staining kit (Arcturus Bioscience) or anti-F4/80 mAb (BD Pharmingen). The F4/80$^+$ cells clustered at the serosal surface of the transmural ulcer of the colon were collected by use of the laser capture microdissection system (PixCell IIe LCM System; Arcturus Bioscience) to obtain an RNA fraction using the PicoPure RNA Isolation kit (Arcturus Bioscience).

RT-PCR

Total RNA isolated from cells and organs was subjected to RT-PCR. Primer structures are shown in Table I. Real-time quantitative PCR analysis was performed using a SYBR Green PCR Master Mix (Applied Biosystems) and the ABI 7700 Sequence Detector System (Applied Biosystems). Expression of mRNA was normalized to the levels of the GAPDH

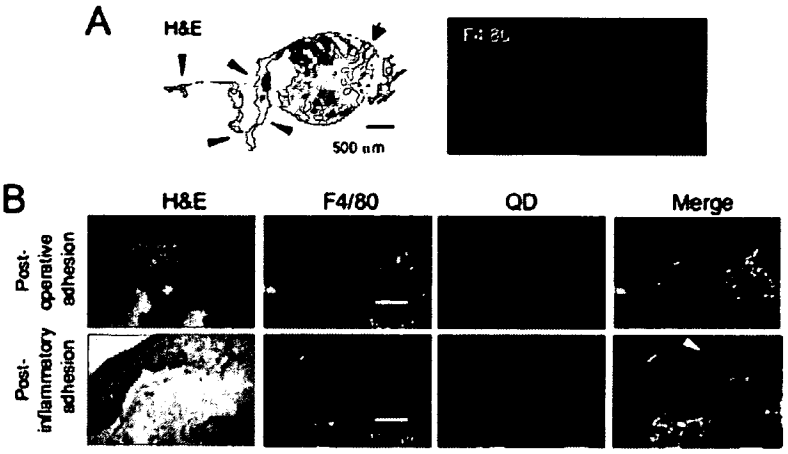

FIGURE 1. PMϕ form aggregates at the site of postoperative and postinflammatory peritoneal adhesions. *A*, Frozen sections prepared from peritoneal adhesions to ischemic buttons (postoperative model) were assessed. The serial sections were stained with H&E and with anti-F4/80 mAb. An arrow and arrowheads indicate the ischemic button and adhesive omentum, respectively. *B*, Frozen sections were prepared from peritoneal adhesions to ischemic buttons (postoperative model) or to the colon after induction of colitis (postinflammatory model) and subjected to H&E staining and immunostaining with anti-F4/80 mAb (green). The PMϕ (1×10^6) obtained from naive mice were labeled with QD (red) and i.p. transferred at the initiation of adhesions. Two images were overlaid in the merged image. Representative pictures from five mice in each experiment are shown. Bars represent 100 μm. Arrowhead indicates mucosal infiltration of Mϕ that does not contain QD-labeled PMϕ.

mRNA expressed. The step-cycle program was set for denaturing at 95°C for 15 s, annealing at 60°C, and extension at 72°C for 45 s, for a total of 40 cycles.

Chemotaxis assay

Aliquots of PMϕ or BMϕ (1×10^7 cells/ml) were prestained for 30 min at 37°C with 3 μg/ml 3′-*O*-Acetyl-2′,7′-bis(carboxyethyl)-4 or 5-carboxyfluorescein, diacetoxymethyl ester (Molecular Probes) and then suspended at 1×10^6 cells/ml in DMEM containing 0.5% BSA and 20 mM HEPES. A chemotaxis assay was performed using a Chemo Tx-96 Chemotaxis Plate (NeuroProbe), as follows. Pretreatment of cells was performed by incubation with or without 50 ng/ml CCL1 for 4 h. Enhanced expression of CCR8 in CCL1-treated PMϕ at this time point was confirmed by flow cytometry. After washing, 65 μl of cell suspension was loaded onto the membrane plate and placed onto a flat-bottom microtiter plate with 96 wells containing 30 μl of serially diluted CCL1 solution in each well. The plate was then incubated at 37°C for 90 min and cells which had undergone migration were collected. These collected cells were counted using a fluorescence microplate reader (FluoroScan Ascent FL; Labsystems). Some experiments were performed in the presence of pertussis toxin (PTX; Calbiochem).

ELISA for CCL1 secretion into peritoneal cavity

To determine the levels of CCL1 in the peritoneal cavity, we collected peritoneal lavage fluid. PBS (1.5 ml) was injected into the peritoneal cavity of mice with or without TNBS-induced colitis as described below, and 1.2–1.4 ml of fluid was recovered. After clearing by centrifugation, the level of CCL1 was determined using paired Abs (Ab Mab8451 for capture and biotinylated Ab BAF845 for detection; R&D Systems) according to the manufacturer's instructions. Bound Ab was detected with peroxidase-labeled avidin (Sigma-Aldrich) and tetramethyl benzidine was used as the substrate. Sensitivity of this assay was 0.2 ng/ml in our hands.

Chemokine-induced Mϕ aggregation (CIMA) assay

Mouse peritoneal mesothelial cells (PMCs) were isolated from omental tissue as described previously (19, 20). The PMCs (1×10^5 cells/well) were plated and cultured on the collagen-coated 24-well dish until they had reached confluence. The QD-labeled PMϕ were added to PMC cultures at a concentration of 1×10^5 cells/well in 10% FCS-DMEM. After addition of serial dilutions of CCL1 or other stimulants, the plates were incubated at 37°C and examined by fluorescent microscopy at the indicated time points. The formation of aggregates was quantified by capturing and analyzing images using NIH ImageJ (National Institutes of Health, Bethesda, MD). The cell aggregates which occurred in >10-μm^2 areas were picked and the total aggregation area in the field was summed. Three fields in each well were randomly chosen and analyzed.

Prevention of postinflammatory and postoperative peritoneal adhesions

In the colitis-associated adhesion model, anti-CCL1-neutralizing mAb or control rat IgG (150 μg) was administered 1 h before the colonic administration of TNBS. Mice were sacrificed at the indicated time point and the severity of adhesion was evaluated according to a standard scoring system reported previously (6) as follows: 0, no adhesion; 1, one thin filmy adhesion; 2, more than one thin adhesions; 3, thin adhesion with focal point; 4, thick adhesion with plantar attachment or more than one thick adhesion with focal point; 5, very thick vascularized adhesions of more than one plantar adhesion. In some experiments, the removed colon was observed with a Realtime In Vivo MacroImaging System (Relyon) equipped with long passed red-viewing filter (>610 nm wavelength) and a CCD camera (Hamamatsu Photonics). The area of fluorescent red color was extracted using Adobe Photoshop CS2 from captured images and quantified using ImageJ. In a model for postoperative peritoneal adhesions, 150 μg of anti-CCL1 mAb or control rat IgG was administered i.p. immediately after surgery and 3 days later. All mice were sacrificed at day 6 and the severity of adhesions to each ischemic button was scored according to the following system: 0, no adhesion; 1, thin filmy adhesion; and 2, thick planter adhesion.

Statistics

Data are expressed as mean ± SD. Statistical analysis was performed using the Statview II statistical program (Abacus Concepts) adapted for the Macintosh computer. The Student *t*, Tukey Kramer's honestly significant difference and Mann-Whitney *U* tests were used as indicated in the figure legends. Statistical interpretation of the results is indicated in the

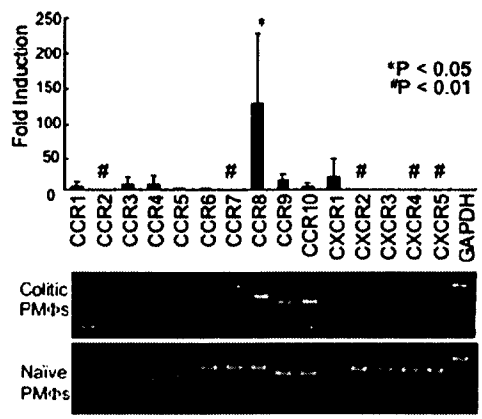

FIGURE 2. Expression of chemokine receptors in PMϕ aggregates at the adhesion after induction of TNBS colitis. Quantitative RT-PCR of cell aggregates obtained with laser capture microdissection from the F4/80$^+$ Mϕ aggregates 24 h after induction of TNBS colitis. Relative expression in aggregates was compared with naive PMϕ for each chemokine receptor as determined by quantitative RT-PCR. Results are shown as an average and 1 SD of four preparations of RNA samples obtained from each of four mice by microdissection. #*, Statistically significant up-regulation or down-regulation from PMϕ samples obtained from four naive mice by the Mann-Whitney *U* test. Representative pictures of PCR products are shown.

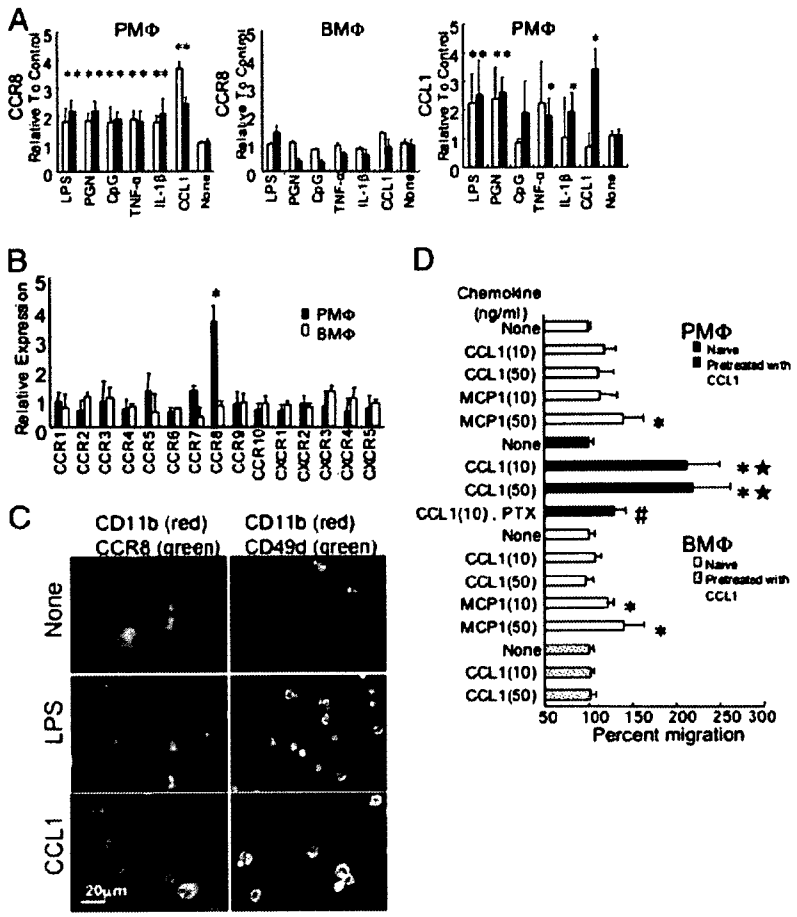

FIGURE 3. In vitro induction of CCR8 and CCL1 expression in PMϕ. *A*, Induction of CCR8 and CCL1 mRNA. PMϕ and BMϕ were stimulated with LPS (100 ng/ml), PGN (1 μg/ml), CpG (1 μg/ml), TNF-α (1 μg/ml), IL-1-β (10 μg/ml), or CCL1 (50 ng/ml) for either 2 (▨) or 4 h (■). Relative expression of mRNA to unstimulated cells was determined by quantitative RT-PCR and the results are shown as mean ± 1 SD of four to six independent cell preparations. *, The difference from unstimulated cells was statistically significant ($p < 0.01$) by the Mann-Whitney *U* test. *B*, Distinct induction of chemokine receptors in PMϕ and BMϕ by CCL1. PMϕ (■) and BMϕ (□) were stimulated with CCL1 (50 ng/ml) for 2 h and relative expression of chemokine receptor mRNA to unstimulated cells was determined by quantitative RT-PCR. Results are shown as mean ± 1 SD of four to six independent cell preparations. *, The difference from unstimulated cell preparations ($n = 6$) was statistically significant ($p < 0.01$) by the Mann-Whitney *U* test. *C*, Induction of surface expression of CCR8 in stimulated PMϕ. The PMϕ were incubated with 50 ng/ml CCL1 or 100 ng/ml LPS and stained with anti-CD11b mAb (red) to visualize the Mϕ cell membrane and with anti-CCR8 pAb (green) after 12 h or anti-CD49d mAb (green) after 48 h. *D*, Chemotaxis of PMϕ and BMϕ in response to CCL1. The PMϕ and BMϕ were pretreated with or without 50 ng/ml CCL1 for 4 h, washed, and subjected to the chemotaxis assay using CCL1 or MCP1 at indicated concentrations. ▨, PMϕ without pretreatment; ■, PMϕ pretreated with CCL1; □, BMϕ without pretreatment; ⊡, BMϕ pretreated with CCL1. Results were shown as mean ± 1 SD of three independent cell preparations. *, Differences from random migration without chemokine (MCP1(50) ▨ vs none ▨, CCL1(10/50) ■ vs none ■, and MCP1(10/50) □ vs none □) were statistically significant ($p < 0.01$); #, difference from chemotaxis without PTX (CCL1, PTX ■ vs CCL1(10/50) ■) was statistically significant ($p < 0.01$). ★, The difference from PMϕ without pretreatment (CCL1(10/50) ■ vs CCL1(10/50) ▨) or the difference from BMϕ (CCL1(10/50) ■ vs CCL1(10/50) ⊡) with the same pretreatment and chemokine concentration was statistically significant ($p < 0.01$). The statistical significance was determined by the Tukey Kramer's honestly significant difference test based on two-factorial ANOVA.

figure legends. Differences were considered statistically significant when $p < 0.05$.

Results

PMϕ trafficking in postoperative and postinflammatory peritoneal adhesions

We first used a postoperative peritoneal adhesion model where peritoneal ischemic buttons were induced by grasping and ligation of the parietal peritoneum. In this system, peritoneal adhesions were constantly formed within 6 days following the operation (17). Cells at the site of adhesion included neutrophils, $CD3^+$ lymphocytes, and $CD11c^+$ cells as reported previously (4–6); however, the infiltration of these cells was rather scattered. In contrast, we found that $F4/80^+$ PMϕ formed their own large aggregates (Fig. 1). In the TNBS hapten-induced colitis model, perforating colonic ulcers were constantly formed and always associated with the adhesions to adjacent tissue. We also found that adhesions to the colon were associated with the presence of Mϕ aggregates at the serosal side (Fig. 1*B*).

To investigate the possibility that PMϕ actually represent the source of these aggregating cells associated with peritoneal adhesions, we labeled naive PMϕ with fluorescent nanocrystal QDs and transplanted them into the peritoneal cavity of mice. QD-labeled PMϕ transferred to peritoneal cavity of naive mice resided in the omentum 24 h after transfer (data not shown). When QD-labeled PMϕ were transferred at the time of induction of postoperative or postinflammatory peritoneal adhesions, they accumulated in the cell aggregates at the serosal site of adhesions and perforating ulcers

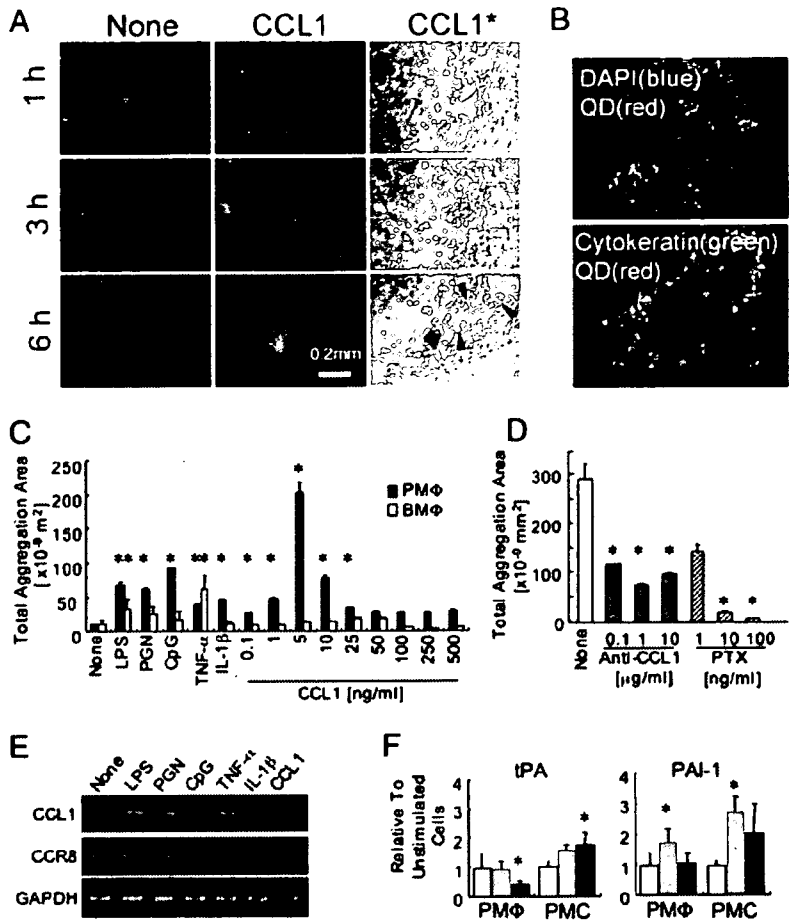

FIGURE 4. Chemokine-induced aggregate formation of PMϕ on monolayers of PMCs (CIMA assay). *A*, QD-labeled pooled PMϕ were placed on the PMC monolayer and stimulated with CCL1 (10 ng/ml) for 1, 3, and 6 h. Pictures are shown for one of three independent experiments with similar results. *, This column shows pictures taken under visible light, which were identical samples as the column using CCL1. Arrowheads indicate the traces of the detached PMC monolayer. *B*, Cell aggregates involve PMCs. The CCL1-induced, QD (red)-labeled PMϕ aggregates as in *A* were collected under a stereomicroscope after 24 h of incubation. Frozen sections were prepared and stained with 4,6 diamidino-2-phenylindole (DAPI, blue, *top*) or with anti-pancytokeratin Ab (green, *bottom*). Original magnification, ×400. *C*, Quantification of CIMA assays. The PMϕ (■) or BMϕ (□) were cultured on PMC monolayers with inflammatory stimulants at the concentrations described in the legend of Fig. 3*A* or at various concentrations of CCL1 for 24 h. The areas of aggregation in captured images were measured. Data are the mean aggregation area ± 1 SD of triplicate experiments. *, Statistically significant differences from cells without stimulation ($p < 0.01$) by the Student *t* test. *D*, Inhibitory effect of anti-CCL1-neutralizing mAb and PTX on aggregate formation. Coculture of PMϕ and PMCs was stimulated with 5 ng/ml CCL1 for 24 h in the presence of various concentrations of inhibitors. Data are the mean aggregation area ± 1 SD of triplicate experiments. *, The difference from controls (without anti-CCL1 mAb, blank column) were statistically significant ($p < 0.01$) by the Student's *t* test. *E*, Expression levels of CCL1 and CCR8 in PMCs after addition of proinflammatory stimuli or CCL1. The PMCs were incubated with stimulants at the concentrations described in the Fig. 3*A* legend or 50 ng/ml CCL1 for 6 h, and subjected to RT-PCR for CCL1 and CCR8. One representative result from four experiments, all giving an identical result, is shown. *F*, CCL1 altered expression of tPA and PAI-1. PMϕ and PMCs were left without stimulation (□) or stimulated with 50 ng/ml CCL1 for either 2 (▨) or 4 (■) h and subjected for quantitative RT-PCR. Results are the mean relative expression when compared with unstimulated cells ± 1 SD of six RNA preparations. *, Statistically significant difference from cells without stimulation ($p < 0.05$) by the Student *t* test.

(Fig. 1*B*). However, the cell infiltrates into the inflamed colonic wall hardly contained QD-labeled cells (Fig. 1*B*, arrowhead). These results indicated that peritoneal adhesions were associated with the massive recruitment of PMϕ to the serosal membrane.

Specific-induction chemokine receptors in PMϕ

To clarify the mechanism of aggregation of PMϕ, we next investigated the chemokine receptor expression patterns in PMϕ aggregates at the serosal surface of the inflamed colon using laser capture microdissection. In contrast to expression of mRNA for all chemokine receptors examined in naive PMϕ, aggregating F4/80$^+$ cells expressed only limited numbers of receptors, i.e., CCR8, CCR9, and CCR10 (Fig. 2). The results of real-time RT-PCR revealed that expression of mRNA for CCR8 was specifically high in aggregated cells (Fig. 2). Expression of CCR8 in serosal-aggregated PMϕ was also confirmed by immunohistological staining in both colitis and postoperative models (data not shown).

Up-regulation of CCR8 in PMϕ is induced by proinflammatory stimuli and by CCL1

We next investigated what types of stimuli might up-regulate mRNA for CCR8 in PMϕ. We found that significant up-regulation of CCR8 mRNA in PMϕ was induced by bacterial components, including LPS, PGN, and CpG, and by the proinflammatory cytokines TNF-α and IL-1-β (Fig. 3*A*). Notably, obvious up-regulation of CCR8 mRNA was induced by CCL1, the ligand for CCR8. In contrast, this degree of CCR8 mRNA up-regulation was not induced in BMϕ by any of stimuli tested (Fig. 3*A*). Up-regulation of

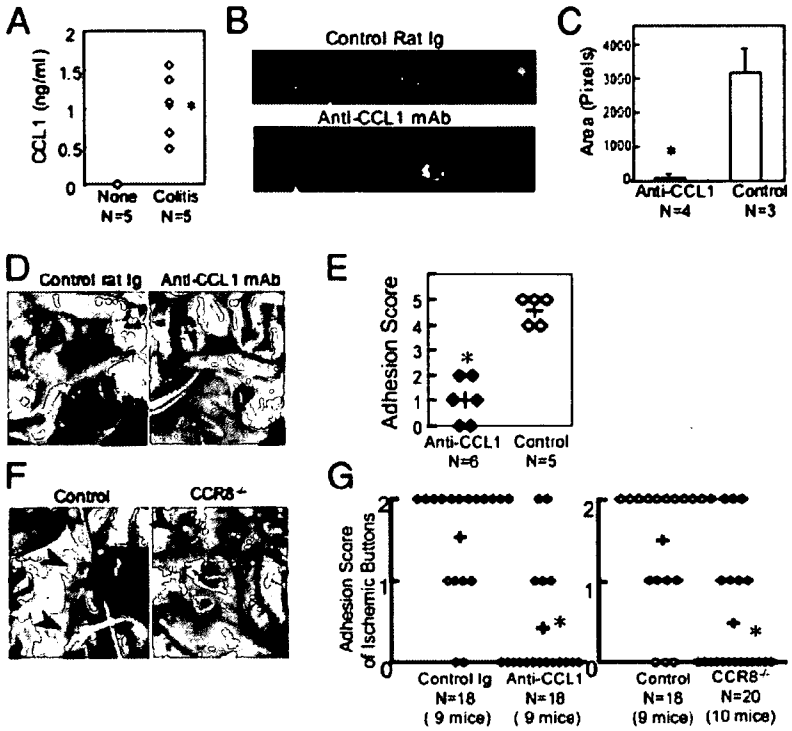

FIGURE 5. The anti-CCL1-neutralizing mAb prevented postinflammatory and postoperative peritoneal adhesions. *A*, Secretion of CCL1 in the peritoneal cavity after induction of colonic inflammation. Peritoneal lavage fluid obtained from naive mice or mice 24 h after induction of colitis with TNBS was subjected to CCL1 ELISA. CCL1 was below the detection limit (0.2 ng/ml) in all five naive mice. The difference was statistically significant ($p < 0.008$) by the Mann-Whitney *U* test, when the values from the naive mice were estimated as 0.2 ng/ml. *B*, Aliquots of QD-labeled (red) PMϕ (2.5×10^5 cells) were transferred to naive C57BL/6J mice on day −1. Next, rat anti-CCL1 mAb (150 μg) or the same amount of control rat IgG Ab were given i.p. and TNBS colitis was induced on day 0. Adhesive tissues in the colon were carefully cut and whole colonic tissues were obtained on day 1. Fluorescent images were superimposed to the pictures under visible light. Representative pictures from each group are shown. *C*, Quantification of QD-labeled cells migrated to the colonic surface. Red colored area in the fluorescent images as in *B* was measured. Results are shown as the mean ± 1 SD. *, Statistically significant difference from control mice ($p < 0.05$) by the Mann-Whitney *U* test. *D*, Anti-CCL1 mAb prevented postinflammatory peritoneal adhesions. Mice were given anti-CCL1 mAb (150 μg) or the same amount of control rat IgG 2 h before the induction of TNBS colitis. Four days later, peritoneal adhesion to the colon was assessed. Representative photos of the colon are shown. The arrows indicate multiple tissue adhesions to the colon in a control Ig-treated mice. Arrowheads indicate colon. *E*, Adhesion scores of mice treated with anti-CCL1 mAb. +, The average value. *, Statistically significant difference from control mice ($p < 0.01$) by the Mann-Whitney *U* test. *F*, Peritoneal adhesions to ischemic buttons were seen 6 days after the operation in control wild-type but not in CCR8$^{-/-}$ mice. The arrowheads indicate ischemic buttons. Typical thick planter adhesion to liver and omentum onto each ischemic button was seen in control mice, but not in CCR8$^{-/-}$ mice. *G*, Adhesion scores of postoperational adhesion in mice treated with control IgG or anti-CCL1 mAb (*left*). *Right panel*, Comparison of wild-type (control) and CCR8$^{-/-}$ mice. Adhesion score for each individual ischemic button was assessed. +, The average value. *, Statistically significant difference from control mice without stimulation ($p < 0.001$) by the Mann-Whitney *U* test.

CCL1 mRNA was also induced in PMϕ by LPS, PGN, TNF-α, IL-1β, and CCL1 itself (Fig. 3*A*). A 3-fold increase of CCL1 in PMϕ cultures stimulated with LPS was also detected by ELISA (data not shown).

Specific up-regulation of CCR8 in various chemokine receptors was seen in PMϕ treated with CCL1. In contrast, CCL1 did not induce particular chemokine receptors in BMϕ (Fig. 3*B*). Immunostaining for CCR8 after stimulation with CCL1 or LPS showed up-regulated expression of CCR8 in the PMϕ together with enhanced expression of the integrin CD49d (Fig. 3*C*), an adhesion molecule which had been reported to be expressed at the site of adhesions (21). Furthermore, we confirmed the function of CCL1-induced CCR8 in PMϕ using a chemotaxis assay. Pretreatment with CCL1 at the concentration of 50 ng/ml caused specific chemoattractive activity for PMϕ to CCL1. In contrast, the responses by BMϕ or untreated PMϕ to CCL1 were poor, although untreated BMϕ and PMϕ responded to MCP1 (Fig. 3*D*). CCL1-induced chemotaxis was inhibited by anti-CCL1 mAb as well as by PTX, which confirmed involvement of a G protein-coupled 7 transmembrane receptor such as CCR8 (Fig. 3*D*). Thus, under conditions where intestinal or peritoneal injury and inflammation occurs, there is a strong and specific positive feedback system to induce the CCL1/CCR8 chemokine system for the recruitment of PMϕ.

CIMA assay: an in vitro model for PMϕ aggregate formation and peritoneal adhesions

Our next experiments were directed to determine whether we could reconstitute aggregate formation of PMϕ associated with adhesions in vitro. When QD-labeled PMϕ were placed on a monolayer of mouse PMCs, PMϕ adhered to PMCs loosely and retained a rounded shape. Addition of CCL1 to this mixed culture led to formation of QD-positive cell aggregates with diameters of >100 μm by 3 h and at later time points (Fig. 4*A*). Importantly, the aggregates involved PMCs. The PMCs became detached from the culture plates and moved into the Mϕ cell aggregates to form a larger mass as shown by the presence of cells, which were QD negative but positively stained with an anti-cytokeratin pAb as a marker for PMCs (Fig. 4, *A* and *B*). Because the surface of the peritoneal cavity, including the omentum and viscera, are covered with mesothelial cells, this result suggests that organs and tissues could be pulled onto Mϕ aggregates via mesothelial cells to eventually form adhesions. In the absence of PMϕ, addition of CCL1

to the PMC layer did not induce detachment or morphological changes (data not shown). The PMϕ also formed aggregates in the presence of bacterial components including LPS, PGN, and CpG, and proinflammatory cytokines, TNF-α and IL-1-β (Fig. 4*C*). The optimal concentration of CCL1 for forming aggregates was ~5–10 ng/ml (Fig. 4*C*). This indicated that the concentration gradient of CCL1 made through this CCL1/CCR8 autocrine system of PMϕ was required for cell migration to form aggregates (Fig. 4*B*). At the high concentration in this one-chamber culture system, the concentration gradient around the cells would not be formed, even if cells produce CCL1. In contrast, BMϕ failed to form CCL1-induced aggregates on PMCs, although they responded to LPS and TNF-α to some extent (Fig. 4*C*). This CCL1-induced aggregate formation was significantly blocked by addition of anti-CCL1-neutralizing mAb or PTX (Fig. 4*D*). Because involvement of PMCs in the PMϕ aggregates was now established, we next investigated the responses of PMCs to CCL1. Although mRNA for CCL1 in unstimulated PMCs was hardly detected, LPS, PGN, TNF-α, IL-1β, and CCL1 induced dramatic up-regulation of CCL1 (Fig. 4*E*). CCR8 was constantly expressed on PMCs and expression level did not change with these stimuli (Fig. 4*E*). Thus, our in vitro model reproduced the initial steps in aggregate formation of PMϕ-enfolding PMCs and demonstrated that PMCs also facilitated the CCL1/CCR8-positive feedback system in PMϕ.

Furthermore, many studies have shown that early fibrinolytic events in the peritoneum play a central role in adhesion formation (1). To investigate possible involvement of CCL1 in the fibrinolytic pathway, mRNA levels for tissue-type plasminogen activator (tPA) and plasminogen activator inhibitor 1 (PAI-1) in the PMϕ and PMCs were assessed. Considerable levels of mRNA for tPA and PAI-1 were detected in unstimulated PMCs and PMϕ (data not shown). In PMϕ, expression of tPA was down-regulated, while that of PAI-1 was up-regulated 2 h after stimulation with CCL1 (Fig. 4*F*). In PMCs, significant up-regulation of PAI-1 was seen 2 h after starting treatment with CCL1 (Fig. 4*F*). Moderate up-regulation of tPA in PMCs became statistically significant when they were treated with CCL1 for 4 h. This CCL1-induced down-regulation of tPA in PMϕ and early up-regulation of PAI-1 in PMϕ and PMCs may also participate in the promotion of cell aggregation and adhesion formation.

Disruption of CCL1/CCR8 interaction prevents peritoneal adhesions

The establishment of a role for CCL1 in an in vitro model of cellular aggregate formation prompted us to investigate the effects of disruption of the CCL1/CCR8 system in vivo. Measurement of the levels of CCL1 in peritoneal lavage fluid revealed that CCL1 was significantly increased in mice with TNBS-induced colitis (Fig. 5*A*). Then, we found that the anti-CCL1-neutralizing mAb efficiently inhibited the formation of aggregates of QD-labeled PMϕ to the colonic serosa after induction of colitis (Fig. 5, *B* and *C*). Four days after induction of TNBS colitis, treatment with anti-CCL1 mAb caused less peritoneal adhesions when compared with mice treated with control rat IgG (Fig. 5, *D* and *E*). In our post-operative adhesion model, two ischemic buttons were created on both sides of the parietal peritoneum. Mice in the control group formed membranous thick adhesions to most of the ischemic buttons (Fig. 5*F*). In contrast, treatment with anti-CCL1 mAb efficiently reduced these adhesions (Fig. 5*G*). Frequency of adhesion formation in $CCR8^{-/-}$ mice was also decreased to the levels comparative to the mouse group treated with anti-CCL1 mAb (Fig. 5, *F* and *G*). Of note, blocking the CCL1-CCR8 interaction did not affect the healing of the initial operative incision.

Discussion

Little is known about cell trafficking between the peritoneal cavity and the organs of this locale including the gastrointestinal tract. We describe here for the first time the migration and aggregate formation of PMϕ at the site of injury. We have revealed the mechanism for this aggregate formation; a specific positive feedback system in PMϕ of the chemokine CCL1 and its receptor CCR8 when tissue damage or infection occurs. We have further established here an in vitro model for aggregation of PMϕ and PMCs, which was triggered by this same CCL1/CCR8 system. Finally, we were able to interrupt the migration of PMϕ and development of subsequent peritoneal adhesions by abrogating CCL1/CCR8 interaction. Each of these significant new findings is discussed in detail in the following paragraphs.

Practically no attention has been given to the serosal cell response in inflammatory disease of visceral organs. However, the damage and injury to viscera reaching the peritoneum is often fatal. In the case of murine colitis, we found that PMϕ form specific aggregates at the site of transmural ulcers and do not migrate into the inflamed colon. It is reasonable that these cell aggregates physically cover this tissue defect in the intestine and maintain a barrier to prevent further exposure to the flora, potential pathogens, or intoxicants. Apparently, the localization and function of PMϕ is distinct from other types of Mϕ, which are recruited directly from the bone marrow via the blood circulation and diffusely infiltrate into the mucosal and submucosal layer of the colon. This unique function of PMϕ is largely mediated through the restricted expression of a specific chemokine and its receptor. Naive PMϕ are responsive to many chemokines; however, PMϕ stimulated with CCL1 specifically up-regulate the expression of CCR8, which then facilitated the development of cell aggregates at this particular site of tissue damage.

The recruitment of PMϕ to the inflamed colonic serosa was dramatic. This was most probably explained by a specific and positive feedback system of CCL1/CCR8 in the PMϕ that we found here. In the case of transmural damage in the colon where normal flora reside, each stimulant positively induced up-regulation of the CCL1/CCR8 system in PMϕ. Because TNBS colitis induced in C57BL/6 mice was ameliorated by the administration of anti-CCL1 mAb (our unpublished data), there may be various inflammatory pathways downstream of CCL1 up-regulation. Previous reports showed that CCL1 functions as a migration inducer of Th2-type cells in both humans and mice (22, 23) as well as neutrophil Mϕ (24). Recent studies demonstrated that CCR8 was expressed in $CD4^+CD25^+$ T cells with IL-10 production (25) or FOXP3 expression (26). In addition, CCL1 was produced by a type of M2 (alternatively activated, M2b) Mϕ (27). Furthermore, rhadinovirus-transformed human T cells produced CCL1 with expression of CCR8, which supported cell growth and cytokine production (28). It is of interest that monocyte-derived dendritic cells use CCR8 in their migration to lymph nodes (29) and Langerhans-type dendritic cells in the skin also produced CCL1 when stimulated with various bacterial components (30). In humans, CCR8 is also expressed in vascular smooth muscle cells and mediates their chemotaxis (31). CCR8 was shown to play a significant role after bacterial challenge in the abdominal cavity in mice (32). However, autoinduction of the receptor CCR8, shown in our results, has not been clearly described to occur in any of these past studies. This vigorous autoactivation system is unique for PMϕ and may explain the rapid and massive recruitment of PMϕ into the injured viscera. This characteristic formation of aggregates by PMϕ certainly plays a key role in the immune system of the peritoneal cavity.

The reaction of PMϕ described here is a very effective defense system; however, in the case of surgical stress or chronic inflammation, we assumed that the reaction of PMϕ to serosal injury might represent a harmful mechanism that ultimately results in severe peritoneal adhesions. To address this notion, we first succeeded in the reconstruction of adhesions between PMϕ and PMCs in vitro. To our surprise, addition of only CCL1 to cocultures of PMCs and PMϕ induced the formation of large cell aggregates. Of interest, we found that mesothelial cells also showed striking up-regulation of CCL1 after various inflammatory conditions including incubation with CCL1 itself. When the intestinal damage reaches the serosal layer, mesothelial cells are exposed to bacterial components or inflammatory cytokines. At this point, CCL1 is first produced locally by mesothelial cells, where it initiates the recruitment and brisk activation of the CCL1/CCR8 system in PMϕ to support their migration and formation of cell aggregates. Furthermore, the enhanced expression of integrin molecules during the aggregate formation of PMϕ as well as up-regulation of PAI in PMCs and down-regulation of tPA in PMϕ via the CCL1/CCR8 system supports the significance of this chemokine system for promotion of further cell aggregation and adhesions, and finally for induction of firm fibrous adhesion tissue. Previous study described the role of T cells in the formation of adhesions (6, 7). Our experiment using T cell-deficient mice also indicated partial involvement of T cells in adhesion formation, however, CCL1-exposed PMϕ did not show enhanced production of TNF-α, IL-6, IL-4, or IL-10 (our unpublished data). The mechanism of the T cell activation along with the CCL1-driven PMϕ recruitment requires further investigation.

In the postoperative model, blockade of the CCL1/CCR8 interaction either with anti-CCL1 mAb or disruption of the *CCR8* gene decreased peritoneal adhesions, but did not affect the healing of the initial midline incision. This suggests a specific effect by blocking the CCL1/CCR8 interaction and points to the possible importance for use of CCL1/CCR8 antagonists to prevent postoperative adhesions without affecting wound healing. Currently, many clinical trials and experimental studies for prevention of peritoneal adhesions have been based upon the idea of modification of the fibrinolytic pathway (33) or the placement of chemical (34) or physical barriers (35, 36). Physical barrier placement was effective in preventing adhesions between viscera and the peritoneal wall; however, it failed to prevent adhesions between viscera. Antiadhesion treatments also includes antibiotics (37), the neurokinin 1 receptor antagonist (17), or cyclooxygenase-2 inhibitors (38, 39) which are mostly nonspecific anti-inflammatory regimen. In contrast, specific blocking of CCL1/CCR8 inhibited the aggregation of PMϕ but would not block the diffuse infiltration of BMϕ into the inflamed site, for the lack of CCR8. This feature suggests the advantage of targeting CCL1/CCR8 for prevention of adhesions, a procedure which would not affect mucosal or systemic defense systems or the wound healing process. Furthermore, we newly developed the CIMA assay in this study. It is now possible to select suitable molecules for use in prevention of peritoneal adhesions in combination of our CIMA assay and high throughput screening of CCR8 antagonists. We now provide a novel target to prevent excess inflammatory responses in the peritoneal cavity and also point to the possibility of prevention of postoperative peritoneal adhesions by blocking CCL1/CCR8 using Abs or antagonists.

Acknowledgment

We thank Dr. Tetsuya Hisoue at International Medical Center of Japan for advice on statistical analysis.

Disclosures

The authors have no financial conflict of interest.

References

1. Saed, G. M., and M. P. Diamond. 2004. Molecular characterization of postoperative adhesions: the adhesion phenotype. *J. Am. Assoc. Gynecol. Laparosc.* 11: 307–314.
2. Ellis, H., B. J. Moran, J. N. Thompson, M. C. Parker, M. S. Wilson, D. Menzies, A. McGuire, A. M. Lower, R. J. Hawthorn, F. O'Brien, et al. 1999. Adhesion-related hospital readmissions after abdominal and pelvic surgery: a retrospective cohort study. *Lancet* 353: 1476–1480.
3. Holmdahl, L. 1999. Making and covering of surgical footprints. *Lancet* 353: 1456–1457.
4. Ellis, H., W. Harrison, and T. B. Hugh. 1965. The healing of peritoneum under normal and pathological conditions. *Br. J. Surg.* 52: 471–476.
5. Haney, A. F. 2000. Identification of macrophages at the site of peritoneal injury: evidence supporting a direct role for peritoneal macrophages in healing injured peritoneum. *Fertil. Steril.* 73: 988–995.
6. Chung, D. R., T. Chitnis, R. J. Panzo, D. L. Kasper, M. H. Sayegh, and A. O. Tzianabos. 2002. CD4$^+$ T cells regulate surgical and postinfectious adhesion formation. *J. Exp. Med.* 195: 1471–1478.
7. Holsti, M. A., T. Chitnis, R. J. Panzo, R. T. Bronson, H. Yagita, M. H. Sayegh, and A. O. Tzianabos. 2004. Regulation of postsurgical fibrosis by the programmed death-1 inhibitory pathway. *J. Immunol.* 172: 5774–5781.
8. Rodgers, K. E., and G. S. diZerega. 1993. Function of peritoneal exudate cells after abdominal surgery. *J. Invest. Surg.* 6: 9–23.
9. Al'Rajab, A., W. Mileski, J. T. Sentementes, P. Sikes, R. B. Harris, and I. J. Dawidson. 1996. The role of neutrophils in peritoneal adhesion formation. *J. Surg. Res.* 61: 143–146.
10. Day, D. W., J. R. Jass, A. B. Price, N. A. Shepherd, J. M. Sloan, I. C. Talbot, B. F. Warren, and G. T. Williams. 2003. Inflammatory disorders of the small intestine. In *Morson and Dawson's Gastrointestinal Pathology*, 4th Ed. Blackwell Science, Oxford, pp. 272–323.
11. Sheehan, A. L., B. F. Warren, M. W. Gear, and N. A. Shepherd. 1992. Fat-wrapping in Crohn's disease: pathological basis and relevance to surgical practice. *Br. J. Surg.* 79: 955–958.
12. Borley, N. R., N. J. Mortensen, D. P. Jewell, and B. F. Warren. 2000. The relationship between inflammatory and serosal connective tissue changes in ileal Crohn's disease: evidence for a possible causative link. *J. Pathol.* 190: 196–202.
13. Hoshino, A., K. Fujioka, T. Oku, S. Nakamura, M. Suga, Y. Yamaguchi, K. Suzuki, M. Yasuhara, and K. Yamamoto. 2004. Quantum dots targeted to the assigned organelle in living cells. *Microbiol. Immunol.* 48: 985–994.
14. Hoshino, A., K. Hanaki, K. Suzuki, and K. Yamamoto. 2004. Applications of T-lymphoma labeled with fluorescent quantum dots to cell tracing markers in mouse body. *Biochem. Biophys. Res. Commun.* 314: 46–53.
15. Lanotte, M., D. Metcalf, and T. M. Dexter. 1982. Production of monocyte/macrophage colony-stimulating factor by preadipocyte cell lines derived from murine marrow stroma. *J. Cell. Physiol.* 112: 123–127.
16. Merchav, S., and G. Wagemaker. 1984. Detection of murine bone marrow granulocyte/macrophage progenitor cells (GM-CFU) in serum-free cultures stimulated with purified M-CSF or GM-CSF. *Int. J. Cell Cloning* 2: 356–367.
17. Reed, K. L., A. B. Fruin, A. C. Gower, A. F. Stucchi, S. E. Leeman, and J. M. Becker. 2004. A neurokinin 1 receptor antagonist decreases postoperative peritoneal adhesion formation and increases peritoneal fibrinolytic activity. *Proc. Natl. Acad. Sci. USA* 101: 9115–9120.
18. Dohi, T., K. Fujihashi, H. Kiyono, C. O. Elson, and J. R. McGhee. 2000. Mice deficient in Th1- and Th2-type cytokines develop distinct forms of hapten-induced colitis. *Gastroenterology* 119: 724–733.
19. Bittinger, F., C. Schepp, C. Brochhausen, H. A. Lehr, M. Otto, H. Kohler, C. Skarke, S. Walgenbach, and C. J. Kirkpatrick. 1999. Remodeling of peritoneal-like structures by mesothelial cells: its role in peritoneal healing. *J. Surg. Res.* 82: 28–33.
20. Kato, S., Y. Yuzawa, N. Tsuboi, S. Maruyama, Y. Morita, T. Matasuguchi, and S. Matsuo. 2004. Endotoxin-induced chemokine expression in murine peritoneal mesothelial cells: the role of Toll-like receptor 4. *J. Am. Soc. Nephrol.* 15: 1289–1299.
21. Bellingan, G. J., P. Xu, H. Cooksley, H. Cauldwell, A. Shock, S. Bottoms, C. Haslett, S. E. Mutsaers, and G. J. Laurent. 2002. Adhesion molecule-dependent mechanisms regulate the rate of macrophage clearance during the resolution of peritoneal inflammation. *J. Exp. Med.* 196: 1515–1521.
22. Zingoni, A., H. Soto, J. A. Hedrick, A. Stoppacciaro, C. T. Storlazzi, F. Sinigaglia, D. D'Ambrosio, A. O'Garra, D. Robinson, M. Rocchi, et al. 1998. The chemokine receptor CCR8 is preferentially expressed in Th2 but not Th1 cells. *J. Immunol.* 161: 547–551.
23. D'Ambrosio, D., A. Iellem, R. Bonecchi, D. Mazzeo, S. Sozzani, A. Mantovani, and F. Sinigaglia. 1998. Selective up-regulation of chemokine receptors CCR4 and CCR8 upon activation of polarized human type 2 Th cells. *J. Immunol.* 161: 5111–5115.
24. Luo, Y., J. Laning, S. Devi, J. Mak, T. J. Schall, and M. E. Dorf. 1994. Biologic activities of the murine β-chemokine TCA3. *J. Immunol.* 153: 4616–4624.
25. Freeman, C. M., B. C. Chiu, V. R. Stolberg, J. Hu, K. Zeibecoglou, N. W. Lukacs, S. A. Lira, S. L. Kunkel, and S. W. Chensue. 2005. CCR8 is expressed by antigen-elicited, IL-10-producing CD4$^+$CD25$^+$ T cells, which regulate Th2-mediated granuloma formation in mice. *J. Immunol.* 174: 1962–1970.
26. Soler, D., T. R. Chapman, L. R. Poisson, L. Wang, J. Cote-Sierra, M. Ryan, A. McDonald, S. Badola, E. Fedyk, A. J. Coyle, et al. 2006. CCR8 expression

identifies CD4 memory T cells enriched for FOXP3$^+$ regulatory and Th2 effector lymphocytes. *J. Immunol.* 177: 6940–6951.
27. Sironi, M., F. O. Martinez, D. D'Ambrosio, M. Gattorno, N. Polentarutti, M. Locati, A. Gregorio, A. Iellem, M. A. Cassatella, J. Van Damme, et al. 2006. Differential regulation of chemokine production by Fcγ receptor engagement in human monocytes: association of CCL1 with a distinct form of M2 monocyte activation (M2b, type 2). *J. Leukocyte Biol.* 80: 342–349.
28. Tamguney, G., J. Van Snick, and H. Fickenscher. 2004. Autocrine stimulation of rhadinovirus-transformed T cells by the chemokine CCL1/I-309. *Oncogene* 23: 8475–8485.
29. Qu, C., E. W. Edwards, F. Tacke, V. Angeli, J. Llodra, G. Sanchez-Schmitz, A. Garin, N. S. Haque, W. Peters, N. van Rooijen, et al. 2004. Role of CCR8 and other chemokine pathways in the migration of monocyte-derived dendritic cells to lymph nodes. *J. Exp. Med.* 200: 1231–1241.
30. Gombert, M., M. C. Dieu-Nosjean, F. Winterberg, E. Bunemann, R. C. Kubitza, L. Da Cunha, A. Haahtela, S. Lehtimaki, A. Muller, J. Rieker, et al. 2005. CCL1-CCR8 interactions: an axis mediating the recruitment of T cells and Langerhans-type dendritic cells to sites of atopic skin inflammation. *J. Immunol.* 174: 5082–5091.
31. Haque, N. S., J. T. Fallon, J. J. Pan, M. B. Taubman, and P. C. Harpel. 2004. Chemokine receptor-8 (CCR8) mediates human vascular smooth muscle cell chemotaxis and metalloproteinase-2 secretion. *Blood* 103: 1296–1304.
32. Matsukawa, A., S. Kudoh, G. Sano, T. Maeda, T. Ito, N. W. Lukacs, C. M. Hogaboam, S. L. Kunkel, and S. A. Lira. 2006. Absence of CC chemokine receptor 8 enhances innate immunity during septic peritonitis. *FASEB J.* 20: 302–304.
33. Saed, G. M., and M. P. Diamond. 2003. Modulation of the expression of tissue plasminogen activator and its inhibitor by hypoxia in human peritoneal and adhesion fibroblasts. *Fertil. Steril.* 79: 164–168.
34. Yaacobi, Y., A. A. Israel, and E. P. Goldberg. 1993. Prevention of postoperative abdominal adhesions by tissue precoating with polymer solutions. *J. Surg. Res.* 55: 422–426.
35. Becker, J. M., M. T. Dayton, V. W. Fazio, D. E. Beck, S. J. Suyker, S. D. Wexner, B. G. Wolff, P. L. Roberts, L. E. Smith, S. A. Sweeney, and M. Moore. 1996. Prevention of postoperative abdominal adhesions by a sodium hyaluronate-based bioresorbable membrane: a prospective, randomized, double-blind multicenter study. *J. Am. Coll. Surg.* 183: 297–306.
36. Gago, L. A., G. M. Saed, S. Chauhan, E. F. Elhammady, and M. P. Diamond. 2003. Seprafilm (modified hyaluronic acid and carboxymethylcellulose) acts as a physical barrier. *Fertil. Steril.* 80: 612–616.
37. Oncel, M., N. Kurt, F. H. Remzi, S. S. Sensu, S. Vural, C. F. Gezen, T. G. Cincin, and E. Oleay. 2001. The effectiveness of systemic antibiotics in preventing postoperative, intraabdominal adhesions in an animal model. *J. Surg. Res.* 101: 52–55.
38. Katada, J., H. Saito, and A. Ohashi. 2005. Significance of cyclooxygenase-2 induced via p38 mitogen-activated protein kinase in mechanical stimulus-induced peritoneal adhesion in mice. *J. Pharmacol. Exp. Ther.* 313: 286–292.
39. Saed, G. M., A. R. Munkarah, and M. P. Diamond. 2003. Cyclooxygenase-2 is expressed in human fibroblasts isolated from intraperitoneal adhesions but not from normal peritoneal tissues. *Fertil. Steril.* 79: 1404–1408.